Circulation

ORIGINAL RESEARCH ARTICLE

Endothelial-to-Mesenchymal Transition Contributes to Accelerated Atherosclerosis in Hutchinson-Gilford Progeria Syndrome

Magda R. Hamczyk, PhD*; Rosa M. Nevado, PhD*; Pilar Gonzalo, PhD; María J. Andrés-Manzano; Paula Nogales, PhD; Víctor Quesada, PhD; Aránzazu Rosado, BSc; Carlos Torroja, PhD; Fátima Sánchez-Cabo, PhD; Ana Dopazo, PhD; Jacob F. Bentzon, MD, PhD; Carlos López-Otín, PhD; Vicente Andrés, PhD

BACKGROUND: Atherosclerosis is the main medical problem in Hutchinson-Gilford progeria syndrome, a rare premature aging disorder caused by the mutant lamin-A protein progerin. Recently, we found that limiting progerin expression to vascular smooth muscle cells (VSMCs) is sufficient to hasten atherosclerosis and death in *Apoe*-deficient mice. However, the impact of progerin-driven VSMC defects on endothelial cells (ECs) remained unclear.

METHODS: *Apoe*- or *Ldlr*-deficient C57BL/6J mice with ubiquitous, VSMC-, EC- or myeloid-specific progerin expression fed a normal or high-fat diet were used to study endothelial phenotype during Hutchinson-Gilford progeria syndrome–associated atherosclerosis. Endothelial permeability to low-density lipoproteins was assessed by intravenous injection of fluorescently labeled human low-density lipoprotein and confocal microscopy analysis of the aorta. Leukocyte recruitment to the aortic wall was evaluated by en face immunofluorescence. Endothelial-to-mesenchymal transition (EndMT) was assessed by quantitative polymerase chain reaction and RNA sequencing in the aortic intima and by immunofluorescence in aortic root sections. TGFβ (transforming growth factor β) signaling was analyzed by multiplex immunoassay in serum, by Western blot in the aorta, and by immunofluorescence in aortic root sections. The therapeutic benefit of TGFβ1/SMAD3 pathway inhibition was evaluated in mice by intraperitoneal injection of SIS3 (specific inhibitor of SMAD3), and vascular phenotype was assessed by Oil Red O staining, histology, and immunofluorescence in the aorta and the aortic root.

RESULTS: Both ubiquitous and VSMC-specific progerin expression in *Apoe*-null mice provoked alterations in aortic ECs, including increased permeability to low-density lipoprotein and leukocyte recruitment. Atherosclerotic lesions in these progeroid mouse models, but not in EC- and myeloid-specific progeria models, contained abundant cells combining endothelial and mesenchymal features, indicating extensive EndMT triggered by dysfunctional VSMCs. Accordingly, the intima of ubiquitous and VSMC-specific progeroid models at the onset of atherosclerosis presented increased expression of EndMT-linked genes, especially those specific to fibroblasts and extracellular matrix. Aorta in both models showed activation of the TGFβ1/SMAD3 pathway, a major trigger of EndMT, and treatment of VSMC-specific progeroid mice with SIS3 alleviated the aortic phenotype.

CONCLUSIONS: Progerin-induced VSMC alterations promote EC dysfunction and EndMT through TGFβ1/SMAD3, identifying this process as a candidate target for Hutchinson-Gilford progeria syndrome treatment. These findings also provide insight into the complex role of EndMT during atherogenesis.

Key Words: aging ■ atherosclerosis ■ endothelial cells ■ endothelial-mesenchymal transition ■ progeria ■ vascular smooth muscle

Correspondence to: Magda R. Hamczyk, PhD, Departamento de Bioquímica y Biología Molecular, Universidad de Oviedo, Calle Fernando Bongera SN, 33006 Oviedo, Spain, Email hamczykmagda@uniovi.es; or Vicente Andrés, PhD, Laboratory of Molecular and Genetic Cardiovascular Pathophysiology, Centro Nacional de Investigaciones Cardiovasculares Carlos III (CNIC), Calle Melchor Fernández Almagro 3, 28029 Madrid, Spain, Email vandres@cnic.es
*M.R. Hamczyk and R.M. Nevado contributed equally.
Supplemental Material is available at https://www.ahajournals.org/doi/suppl/10.1161/CIRCULATIONAHA.123.065768.
For Sources of Funding and Disclosures, see page 1628.

Circulation is available at www.ahajournals.org/journal/circ

Clinical Perspective

What Is New?

- Progerin-driven vascular smooth muscle cell alterations and death trigger proatherogenic changes in endothelial cells in the aorta.
- Atherosclerotic plaques of progeroid mice are characterized by extensive endothelial-to-mesenchymal transition that emerges as a response to vascular smooth muscle cell damage and frequently gives rise to fibroblast-like cells that retain endothelial features.
- Atherosclerotic plaques of progeroid mice present activation of SMAD3-mediated transforming growth factor β1 pathway that can be targeted in vivo with SIS3 (specific inhibitor of SMAD3).

What Are the Clinical Implications?

- Our preclinical studies in mice with premature aging syndrome indicate that vascular smooth muscle cell alterations might precede and induce endothelial dysfunction and extensive endothelial-to-mesenchymal transition, contributing to atherosclerosis.
- Inhibition of SMAD3-mediated transforming growth factor β1 signaling is a potential therapeutic target for alleviating vascular disease in Hutchinson-Gilford progeria syndrome.

Nonstandard Abbreviations and Acronyms

CDH2	N-cadherin
CNIC	Centro Nacional de Investigaciones Cardiovasculares
EC	endothelial cell
EndMT	endothelial-to-mesenchymal transition
ERG	ETS-related gene
HFD	high-fat diet
HGPS	Hutchinson-Gilford progeria syndrome
LDL	low-density lipoprotein
MAEC	mouse aorta endothelial cell
PDGFRβ	platelet derived growth factor receptor β
PECAM-1	platelet endothelial cell adhesion molecule-1
pSMAD3	phosphorylated SMAD3
PTPRC	protein tyrosine phosphatase receptor type C
SIS3	specific inhibitor of SMAD3
TGF	transforming growth factor
VSMC	vascular smooth muscle cell
VWF	von Willebrand factor

Hutchinson-Gilford progeria syndrome (HGPS) is an extremely rare disease caused by a de novo point mutation in the *LMNA* gene.[1,2] *LMNA* encodes lamin A, a nuclear envelope protein involved in maintaining nuclear structure and function. The most frequent HGPS-causing mutation (c.1824C>T; p.G608G) activates a cryptic splice site in exon 11 in the *LMNA* pre-mRNA, causing aberrant splicing and production of a truncated mutant protein called progerin. Because it lacks 50 amino acids normally present in prelamin A, progerin cannot undergo the normal posttranslational maturation process and remains permanently farnesylated and carboxymethylated. The accumulation of progerin alters multiple cell processes, including the regulation of nuclear shape, gene transcription, signal transduction, DNA damage repair, and cell cycle progression, that accelerate organismal aging.[3] HGPS recapitulates many features of physiological aging, such as reduced bone density, joint stiffness, alopecia, skin wrinkling and mottling, and cardiovascular disease.[4] Arteries in patients with HGPS are severely depleted of vascular smooth muscle cells (VSMCs) and show exaggerated extracellular matrix accumulation, calcification, adventitial thickening, and atherosclerosis.[5–7] Most patients with HGPS die in adolescence from complications of atherosclerosis such as myocardial infarction, heart failure, or stroke.[4,7]

The main risk factor for atherosclerosis is aging, and the disease typically becomes clinically manifest from 50 to 60 years of age.[8] Atherosclerosis has historically been thought of as involving a series of steps, in which each cell type in the arterial wall has a role limited in space and time. In this conventional view, atherosclerosis is initiated by the accumulation of low-density lipoprotein (LDL) in the arterial wall and consequent endothelial cell (EC) activation, events that trigger recruitment of bloodborne leukocytes into the subintimal space. Monocytes in the aortic wall then differentiate into macrophages, which ingest and accumulate LDL, transforming them into foam cells that contribute to atherosclerotic plaque growth. In response to proinflammatory stimuli, medial VSMCs undergo phenotypic switching and migrate towards the neointima, where they proliferate and can generate a fibrous cap below the endothelial monolayer that protects against plaque rupture and its life-threatening consequences, such as myocardial infarction or stroke.[9]

Recent studies have described high cellular heterogeneity and plasticity in healthy and atherosclerotic vessels, suggesting that atherosclerosis is more complex than initially thought.[10] For instance, VSMCs can acquire characteristics reminiscent of foam cells, fibroblasts, and osteochondrogenic cells in the lesions.[9] Moreover, ECs can undergo a transition towards a mesenchymal phenotype, a process known as endothelial-to-mesenchymal transition (EndMT), to give rise to a wide variety of cell types in the lesion, including fibroblasts, osteoblasts, and VSMCs.[11] Likewise, the protective fibrous cap can be

formed by cells of non-VSMC origin.[12] These processes seem to be regulated by crosstalk between VSMCs, ECs, and immune cells.[13,14] These recent discoveries indicate that there is still a gap in current knowledge about the initiation and progression of atherosclerosis. Studies of rare diseases featuring accelerated atherosclerosis, like HGPS, may help to elucidate the complex mechanisms leading to atheroma plaque formation and disruption.

We previously generated and characterized the atheroprone *Apoe*$^{-/-}$*Lmna*$^{G609G/G609G}$ and *Ldlr*$^{-/-}$*Lmna*$^{G609G/G609G}$ HGPS mouse models with ubiquitous progerin expression, which show accelerated atherosclerosis and recapitulate most vascular features present in patients with HGPS.[15,16] We have also demonstrated that VSMC-specific progerin expression is sufficient to cause VSMC loss in the arterial wall, leading to accelerated atherosclerotic lesion formation and death in *Apoe*-deficient mice.[15,17] However, it remained unclear how VSMC-restricted progerin expression triggers the complete vascular manifestation of the disease. Here, we investigated how progerin-induced VSMC alterations affect ECs and the consequences of this cellular crosstalk for atherogenesis.

METHODS

Ethical Statement

Animal experiments conformed to European Union Directive 2010/63EU and recommendation 2007/526/EC, enacted in Spanish law under Real Decreto 53/2013. Animal protocols were approved by the local ethics committees and the Animal Protection Area of the Comunidad Autónoma de Madrid (PROEX76/14, PROEX167/16, PROEX149.0/20) and followed the Animal Research: Reporting of In Vivo Experiments guidelines.[18] Blood for LDL isolation was obtained from healthy volunteers after informed consent in accordance with local ethics committee guidelines (CEI PI 12_2016-v2).

Mice

Mice used in this study were C57BL/6J (JAX Mice Strain) males with ubiquitous, VSMC-, EC-, and myeloid-specific progerin expression and their littermate controls with lamin A/C and lamin C–only expression, respectively (Table S1), all with *Apoe* or *Ldlr* deficiency. Gene expression studies in the aortic intima included males and females (Tables S2 and S3). For establishing mouse aorta endothelial cell (MAEC) cultures, wild-type males were used (without *Apoe* or *Ldlr* deficiency). Mice were housed in a specific pathogen–free facility at the Centro Nacional de Investigaciones Cardiovasculares (CNIC) in individually ventilated cages with 12 hours light/12 hours dark cycle at a temperature of 22 ± 2°C and 50% relative humidity (range, 45%–60%). Mice had ad libitum access to water and food (normal chow diet: 5K67, LabDiet or D184, SAFE or Rod18-A, LASQCdiet). When indicated, 8-week-old mice were placed for 8 weeks on a high-fat diet (HFD) containing 10.7% total fat and 0.75% cholesterol (S9167-E010 or S9167-E011, Ssniff) and euthanized at 16 weeks of age. To induce progerin expression, 6-week-old *Apoe*$^{-/-}$*Lmna*$^{LCS/LCS}$*Cdh5Cre*^{ERT2} and *Apoe*$^{-/-}$*Lmna*$^{LCS/LCS}$ mice received intraperitoneal injections of tamoxifen (T5648, Sigma; 0.2 mg per g body weight) dissolved in corn oil (C8267, Sigma) on 3 alternate days. Except for endothelial permeability studies, whole mount aortic preparations, and coculture of MAECs with aortic media explants, animals were fasted overnight before euthanasia. Mice were euthanized by CO_2 inhalation, except for endothelial permeability studies and whole mount aortic preparations, for which animals were euthanized by general anesthesia followed by intracardiac perfusion with KCl and then with formaldehyde. More details on animal studies are provided in the Supplemental Methods and Data Set S1.

Inhibition of SMAD3 Phosphorylation In Vivo

Specific inhibitor of SMAD3[19] (SIS3; Chemical Abstracts Service number 521984-48-5, 5291, R&D Systems) was dissolved in dimethyl sulfoxide (Chemical Abstracts Service number 67-68-5, A3672, PanReac AppliChem) at a concentration of 100 mg/mL and stored at −80°C (stock solution). On the day of each injection, SIS3 stock solution was thawed and diluted in sterile PBS to a final concentration of 0.5 mg/mL (0.5% dimethyl sulfoxide).

SIS3 (5 mg/kg) or vehicle (0.5% dimethyl sulfoxide in PBS) was administered intraperitoneally to *Apoe*$^{-/-}$*Lmna*$^{LCS/LCS}$ *SM22αCre* and *Apoe*$^{-/-}$*Lmna*$^{LCS/LCS}$ male mice that were previously allocated into treatment and control groups by stratified randomization (each litter formed a stratum; block randomization within each stratum was performed to assign equal or similar numbers of animals from each litter to each group). The researcher administering the SIS3 or vehicle to mice was aware of the treatment group allocation. To confirm SIS3 inhibitory properties, 12-week-old mice received a single injection of SIS3 or vehicle and were euthanized 1, 4, or 24 hours afterwards. To assess therapeutic effects of SIS3, 8-week-old mice received 3 injections per week for 8 weeks and were euthanized at 16 weeks of age.

In Vivo Endothelial Permeability to LDL

Endothelial permeability to LDL was assessed as previously described[20] (Supplemental Methods).

Quantification of Atherosclerosis Burden in Thoracic Aorta

Atherosclerosis burden in the thoracic aorta was assessed as previously described[15,16] (Supplemental Methods).

Histology and Immunofluorescence in Paraffin-Embedded Sections

See Supplemental Methods and Table S4.

Immunofluorescence in OCT-Embedded Sections

See Supplemental Methods and Table S5.

Immunofluorescence in Whole Mount En Face Aorta Preparations

See Supplemental Methods and Table S6.

Collection of Aortic Intimal Cell Lysates and RNA Extraction

RNA from the aortic intima was isolated following a previously described protocol[21] (Supplemental Methods; Figure S1; Tables S2 and S3; Data Set S2).

Reverse Transcription and Quantitative Polymerase Chain Reaction

See Supplemental Methods and Table S7.

RNA Sequencing

See Supplemental Methods and Data Set S2.

Determination of Serum Transforming Growth Factor β1 and β2 Concentration

See Supplemental Methods.

Protein Extraction and Western Blotting

See Supplemental Methods and Table S8.

Determination of Transforming Growth Factor β1 Secreted by the Aortic Medial Layer

See Supplemental Methods.

Primary MAEC Cultures

See Supplemental Methods.

Stimulation of MAECs With Transforming Growth Factor β1

See Supplemental Methods.

Coculture of MAECs With Aortic Media Explants

See Supplemental Methods.

MAEC Immunofluorescence

See Supplemental Methods and Table S9.

Hematology and Serum Cholesterol

See Supplemental Methods.

Data Availability

A detailed description of the methods and materials used in this work is provided in the article and in the online Supplemental Material. Data supporting the findings of this study either are included in the article and online Supplemental Material or can be requested from the corresponding authors. RNA sequencing data are available at the Sequence Read Archive (BioProject accession No. PRJNA1120035) and Gene Expression Omnibus (accession No. GSE269166) repositories of the National Center for Biotechnology Information.

Statistical Analysis

Data distribution was evaluated with the Kolmogorov-Smirnov and D'Agostino-Pearson normality tests. Normally distributed data are presented as the mean (error bars indicate SEM) and were analyzed using a *t* test, applying Welch correction if the groups had unequal variances. Nonnormally distributed data are presented as the median (with interquartile range; error bars indicate minimum and maximum) and were analyzed by Mann-Whitney test. Statistical tests for comparison of 2 groups were 2-tailed except for analyses where the possibility of the relationship in 1 direction was tested (data about the potential therapeutic effects of SIS3 on HGPS-related vascular alterations; primary outcome: atherosclerosis burden). Statistical analysis was performed with Prism 9 (GraphPad). Outliers identified with the GraphPad outlier calculator (www.graphpad.com/quickcalcs/Grubbs1.cfm) were discarded from further analysis (Data Set S1). Differences were considered significant at $P < 0.05$. Descriptive statistics are shown in Data Set S3 for main figures and in Data Set S4 for supplemental figures.

RESULTS

Ubiquitous and VSMC-Specific Progerin Expression Triggers Endothelial Dysfunction in the Aorta

Given that EC dysfunction is a key factor in atherosclerosis initiation, we sought to analyze changes in EC phenotype and function in atheroprone progeroid mouse models. We examined mice with ubiquitous progerin expression (*Apoe*$^{-/-}$*Lmna*$^{G609G/G609G}$) and VSMC-specific progerin expression (*Apoe*$^{-/-}$*Lmna*$^{LCS/LCS}$*SM22αCre*) and their corresponding controls with normal expression of lamin A/C (*Apoe*$^{-/-}$*Lmna*$^{+/+}$) or expressing only lamin C (*Apoe*$^{-/-}$*Lmna*$^{LCS/LCS}$).[15] Because LDL accumulation in the arterial wall plays a key role in the initiation of atherosclerosis, we first assessed in vivo endothelial permeability for LDL particles in normal chow–fed 16-week-old mice, which develop early atherosclerotic disease.[15] Mice received intravenous injections of fluorescently labeled human LDL (Atto565-LDL) and were euthanized 1 hour after the injection, and the aorta was harvested for confocal microscopy analysis (Figure 1A). Aortas from both *Apoe*$^{-/-}$*Lmna*$^{G609G/G609G}$ and *Apoe*$^{-/-}$*Lmna*$^{LCS/LCS}$*SM22αCre* mice showed enhanced endothelial permeability to LDL compared with their control littermates, as revealed by an increased Atto565-LDL–positive area in the aortic arch and thoracic aorta (Figure 1B; negative controls not injected with Atto565-LDL are shown in Figure S2 and Videos S1 through S4). Three-dimensional reconstruction videos confirmed increased Atto565-LDL accumulation on the luminal side of the aortic wall (intima and first layer of the media) in the mutant mice (Figure 1C; Videos S5 through S8).

Immunofluorescence studies in whole mount en face aortic preparations revealed alterations in the size and shape of ECs in both *Apoe*$^{-/-}$*Lmna*$^{G609G/G609G}$ and *Apoe*$^{-/-}$*Lmna*$^{LCS/LCS}$*SM22αCre* mice (Figure 1D). Remarkably, aortic intima in both progeroid models contained cells negative for the EC markers PECAM-1 (platelet endothelial cell adhesion molecule-1 or CD31)[22] and

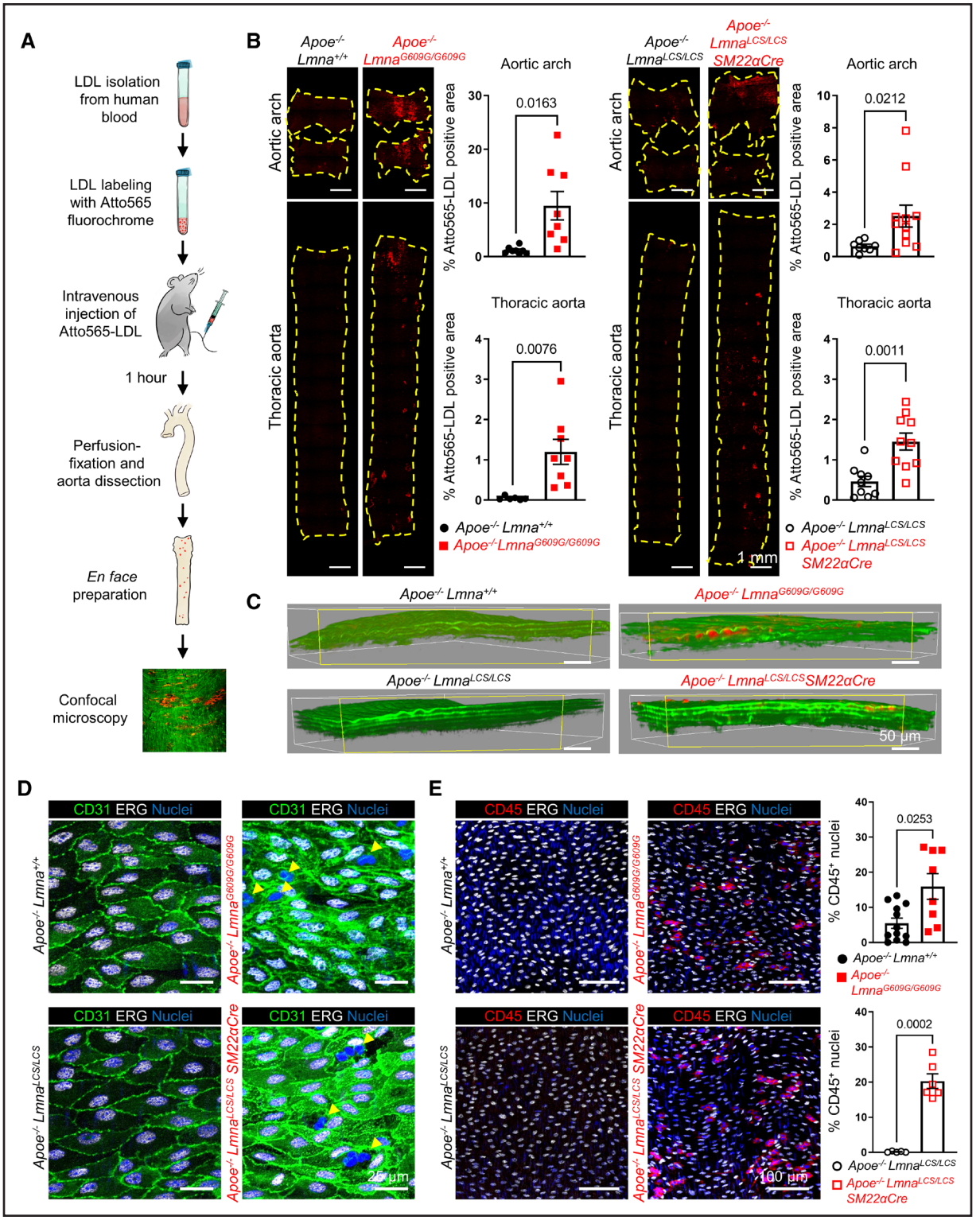

Figure 1. Endothelial dysfunction in aortas of progeroid *Apoe*$^{-/-}$*Lmna*$^{G609G/G609G}$ and *Apoe*$^{-/-}$*Lmna*$^{LCS/LCS}$*SM22αCre* mice.
Male mice fed normal chow were euthanized at 16 weeks of age. **A**, Workflow of in vivo low-density lipoprotein (LDL) permeability experiments. LDL was isolated from blood of healthy human volunteers, labeled with Atto565 fluorescent dye, and injected intravenously into mice (15 µg Atto565-LDL per g of body weight). One hour after the injection, the aorta was pre-fixed by intracardiac perfusion with 4% formaldehyde, excised, cleaned of fatty tissue, opened longitudinally, and pinned out flat on a silicone plate for overnight fixing with 4% formaldehyde. After washing, the aorta was mounted en face on a slide for confocal microscopy analysis. **B**, Representative tile-scan confocal images of whole mount aortas from mice injected with Atto565-LDL (red). Scale bar, 1 mm. Graphs show quantification of endothelial permeability to LDL (as the percentage of red staining in relation to the total marked aortic area) in the aortic arch and thoracic aorta of *Apoe*$^{-/-}$*Lmna*$^{+/+}$ mice (n=6–8), *Apoe*$^{-/-}$*Lmna*$^{G609G/G609G}$ mice (n=8), *Apoe*$^{-/-}$*Lmna*$^{LCS/LCS}$ mice (n=8 or 9), and *Apoe*$^{-/-}$*Lmna*$^{LCS/LCS}$*SM22αCre* mice (n=10 or 11). **C**, Representative still (*Continued*)

Figure 1 Continued. frames from 3-dimentional reconstruction videos (Videos S5 through S8), showing the aortic wall of mice injected with Atto565-LDL (red). Green signal corresponds to elastic-fiber autofluorescence. Scale bar, 50 µm. **D**, Representative immunofluorescence images showing CD31 and ERG expression in whole mount en face mouse aortic preparations. Hoechst 33342 was used to visualize nuclei. Scale bar, 25 µm. Yellow arrowheads indicate cells negative for the endothelial markers CD31 and ERG. **E**, Representative immunofluorescence images showing CD45 and ERG expression in whole mount en face mouse aortic preparations. Hoechst 33342 was used to visualize nuclei. Scale bar, 100 µm. Graphs show leukocyte recruitment quantified as the percentage of CD45-positive nuclei in aortas of *Apoe*$^{-/-}$*Lmna*$^{+/+}$ mice (n=12), *Apoe*$^{-/-}$*Lmna*$^{G609G/G609G}$ mice (n=8), *Apoe*$^{-/-}$*Lmna*$^{LCS/LCS}$ mice (n=5), and *Apoe*$^{-/-}$*Lmna*$^{LCS/LCS}$*SM22αCre* mice (n=6). Data are presented as mean ± SEM together with individual values. Statistical analysis was performed by 2-tailed *t* test with Welch correction, and the *P* values are shown.

ERG (ETS-related gene),[23] a very infrequent observation in control aortas (Figure 1D). Because recruitment of bloodborne leukocytes into the arterial wall is a key process in atherosclerosis initiation and progression, we performed immunofluorescence studies to examine the expression of the canonical leukocyte marker PTPRC (protein tyrosine phosphatase receptor type C or CD45).[24] Analysis of whole mount en face aortic preparations revealed a higher percentage of leukocytes (CD45^{+}CD31^{-}ERG^{-}) adhered to or extravasating through the aortic endothelium (CD45^{-}CD31^{+}ERG^{+}) in both progeroid models than in their control littermates (Figure 1E; Figures S3 and S4; Videos S9 through S12).

Abnormally High Content of Cells Positive for EC Markers in Atheromas of Mice With Ubiquitous and VSMC-Specific Progerin Expression

To examine EC alterations at more advanced atherosclerosis stages, we performed an immunofluorescence analysis of atherosclerotic plaques in the aortic root of 16-week-old progeroid mice with ubiquitous or VSMC-specific progerin expression that had been fed a HFD for the last 8 weeks before euthanasia. As expected, CD31 expression in control *Apoe*$^{-/-}$*Lmna*$^{+/+}$ and *Apoe*$^{-/-}$*Lmna*$^{LCS/LCS}$ mice without progerin expression was predominantly limited to the EC monolayer that separates the atherosclerotic lesion from circulating blood (Figure 2A; Figure S5). In marked contrast, atherosclerotic plaques in both *Apoe*$^{-/-}$*Lmna*$^{G609G/G609G}$ and *Apoe*$^{-/-}$*Lmna*$^{LCS/LCS}$*SM22αCre* mice showed widespread CD31 expression, with diverse localization patterns ranging from scattered individual cells to structures resembling a fibrous cap (Figure 2A; Figure S5). Atherosclerotic lesions in *Apoe*$^{-/-}$*Lmna*$^{G609G/G609G}$ mice also abundantly expressed the EC markers VWF (von Willebrand factor) and ERG, predominantly in CD31-positive zones (Figure 2B and 2C). Elevated CD31 expression was also evident within atheromas in normal chow–fed *Apoe*$^{-/-}$ mice with ubiquitous and VSMC-specific progerin expression at ages close to their maximum survival (21–23 weeks and 51 weeks, respectively; Figure S6). Furthermore, extensive intraplaque CD31, VWF, and ERG staining was observed in *Ldlr*$^{-/-}$*Lmna*$^{G609G/G609G}$ mice (Figure S7), another HGPS-like model featuring accelerated atherosclerosis.[16] These studies demonstrate the abnormal presence of cells with endothelial features inside atherosclerotic plaques in progeroid mice, a phenomenon independent of the genetic modification used to induce atherogenesis (*Apoe* or *Ldlr* deficiency).

Unlike *Apoe*$^{-/-}$*Lmna*$^{G609G/G609G}$ and *Apoe*$^{-/-}$*Lmna*$^{LCS/LCS}$*SM22αCre* mice, *Apoe*$^{-/-}$*Lmna*$^{LCS/LCS}$*Cdh5Cre*^{ERT2} mice with EC-specific progerin expression (Figures S8 through S11) showed neither increased leukocyte recruitment to the aortic intima (Figure S12A) nor augmented CD31 and ERG staining within atheromas (Figure S12B), indicating that endothelial abnormalities observed in progeroid aortas do not stem from progerin expression in ECs. Likewise, *Apoe*$^{-/-}$*Lmna*$^{LCS/LCS}$*LysMCre* mice with progerin expression restricted to myeloid cells[15] did not present CD31 and ERG staining inside atherosclerotic lesions (Figure S13).

Extensive EndMT in Atherosclerotic Lesions in Ubiquitous and VSMC-Specific Progeroid Mice

CD31-positive cells inside atherosclerotic plaques in both *Apoe*$^{-/-}$*Lmna*$^{G609G/G609G}$ and *Apoe*$^{-/-}$*Lmna*$^{LCS/LCS}$*SM22αCre* mice frequently had a mesenchymal-like phenotype rather than a typical EC appearance (Figure 2A; Figure S5), suggesting that ECs in these progeroid mice might undergo EndMT. To test this hypothesis, we optimized a protocol to purify total RNA from the aortic intima (mostly ECs) of normal chow–fed 16-week-old mice with incipient atherosclerosis and examined intimal gene expression by quantitative polymerase chain reaction (Figure 3A). We first quantified the expression of key transcription factors reported to be involved in EndMT. Compared with control mice, the intima layer in both progeroid models expressed higher levels of *Snai1* and *Zeb2* and lower levels of *Snai2* and *Twist1* (Figure 3B). Given the complex relationship between these factors, we integrated the binary logarithm of the fold change ($\log_2$FC) values in a previously reported network model of the molecules involved in the regulation of EndMT.[25] This analysis confirmed the presence of 2 counterbalanced axes modulating EndMT and suggested that the SNAI1-ZEB2 axis is activated and the TWIST1-SNAI2-ZEB1 axis repressed in the endothelium in the initial phases of HGPS-associated atherosclerotic disease (Figure S14).

Additional quantitative polymerase chain reaction analysis of EC-specific genes revealed a significant downregulation of *Pecam1*, *Tek*, and *Cdh5* in the intima of *Apoe*$^{-/-}$*Lmna*$^{LCS/LCS}$*SM22αCre* mice, whereas

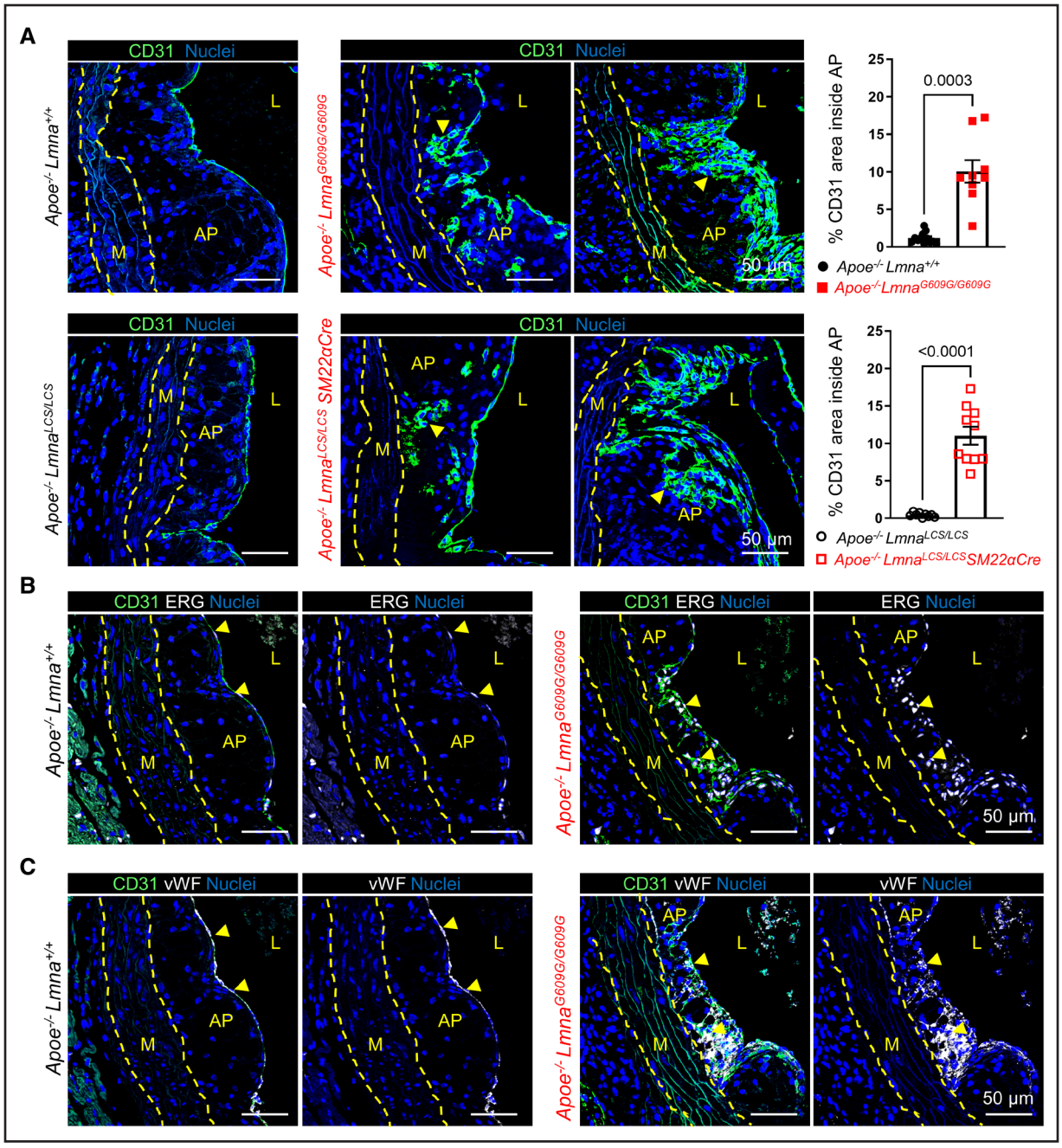

Figure 2. Increased expression of endothelial markers inside atheromas of fat-fed progeroid *Apoe*$^{-/-}$*Lmna*$^{G609G/G609G}$ and *Apoe*$^{-/-}$*Lmna*$^{LCS/LCS}$*SM22αCre* mice.

Starting at 8 weeks of age, male mice were fed a high-fat diet for 8 weeks and then euthanized at 16 weeks of age. Serial sections for immunofluorescence studies were prepared from paraffin-embedded aortic root samples. Representative immunofluorescence images are shown. Hoechst 33342 was used to visualize nuclei. **A**, CD31 expression in atherosclerotic plaques. Yellow arrowheads indicate zones with CD31-positive staining inside atheromas. Graphs show quantification of CD31-positive area inside atheromas (excluding necrotic core and luminal endothelial cells) in *Apoe*$^{-/-}$*Lmna*$^{+/+}$ mice (n=12), *Apoe*$^{-/-}$*Lmna*$^{G609G/G609G}$ mice (n=9), *Apoe*$^{-/-}$*Lmna*$^{LCS/LCS}$ mice (n=9), and *Apoe*$^{-/-}$*Lmna*$^{LCS/LCS}$ *SM22αCre* mice (n=10). **B**, CD31 and ERG expression in atherosclerotic plaques of *Apoe*$^{-/-}$*Lmna*$^{+/+}$ and *Apoe*$^{-/-}$*Lmna*$^{G609G/G609G}$ mice. Yellow arrowheads indicate examples of CD31^{+}ERG^{+} cells. **C**, CD31 and VWF expression in atherosclerotic plaques of *Apoe*$^{-/-}$*Lmna*$^{+/+}$ and *Apoe*$^{-/-}$*Lmna*$^{G609G/G609G}$ mice. Yellow arrowheads indicate examples of CD31^{+}VWF^{+} cells. Data are presented as mean ± SEM together with individual values. Statistical analysis was performed by 2-tailed *t* test with Welch correction, and the *P* values are shown. Scale bar, 50 μm. AP indicates atherosclerotic plaque; L, lumen; and M, media.

the intima of *Apoe*$^{-/-}$*Lmna*$^{G609G/G609G}$ mice only showed significant downregulation of *Tek* (Figure 3C). To identify the cell type to which these ECs were transitioning, we next analyzed the expression of a series of genes previously linked to EndMT that are highly expressed in VSMCs and fibroblasts. This analysis showed elevated

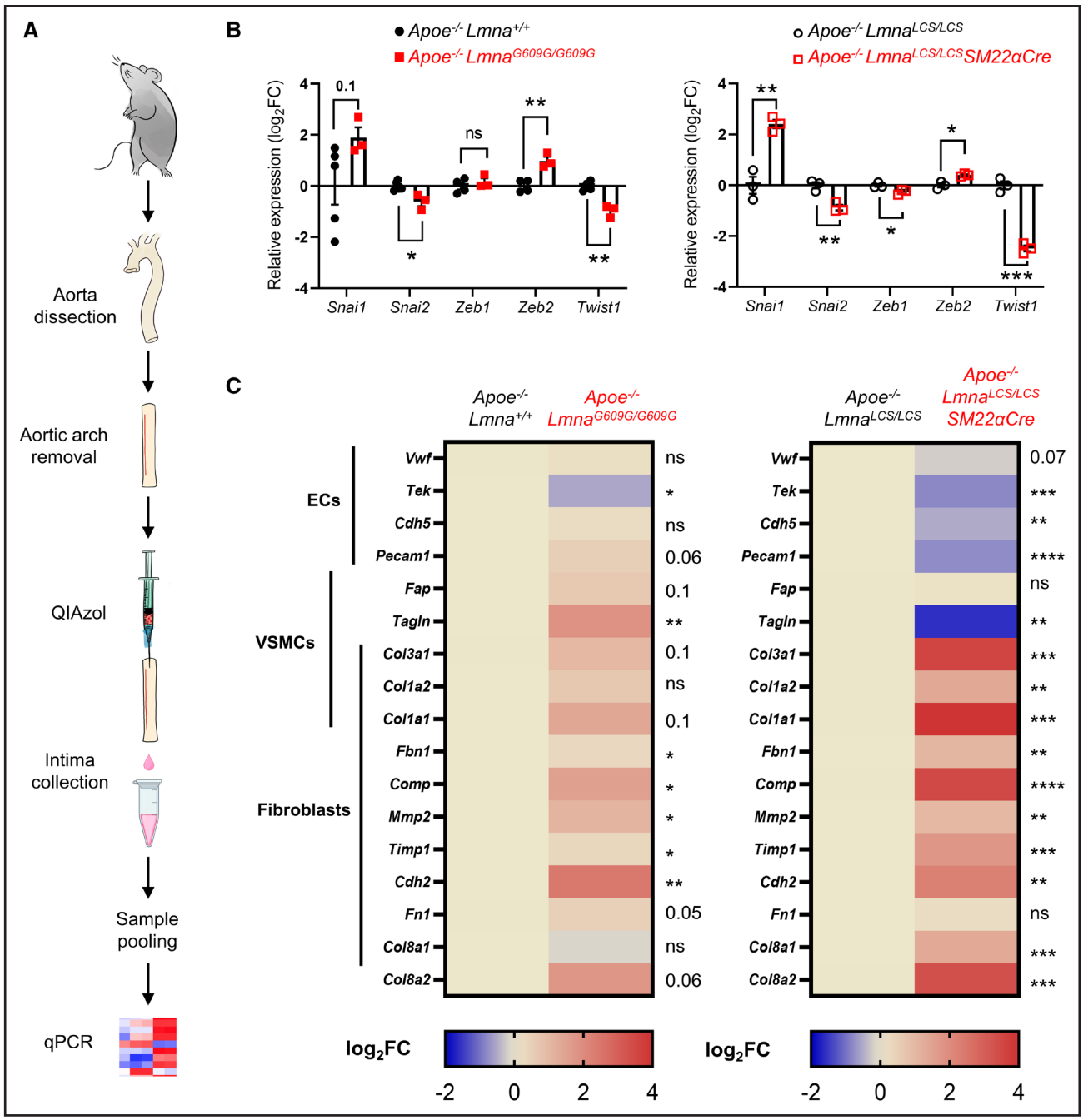

Figure 3. Activation of an endothelial-to-mesenchymal transition (EndMT) transcriptional program in the aortic intima of *Apoe*$^{-/-}$*Lmna*$^{G609G/G609G}$ and *Apoe*$^{-/-}$*Lmna*$^{LCS/LCS}$*SM22αCre* mice.

Male and female mice fed normal chow were euthanized at 16 weeks of age. **A**, Workflow of aortic intima collection for quantitative polymerase chain reaction (qPCR) studies. After euthanasia, mice were perfused intracardially with sterile PBS to remove blood from the aorta. The aorta was then excised and cleaned of fatty tissue, and the aortic arch was discarded. Using a syringe and a needle, QIAzol lysis reagent was slowly passed through the interior of the thoracic aorta, and the resulting intima lysate was collected by gravity in a clean tube. Samples from various animals of the same genotype were pooled for RNA extraction and qPCR analysis of EndMT-related genes. *Hmbs* and *Hprt* genes were used as endogenous controls. **B**, Graphs show *Snai1*, *Snai2*, *Zeb1*, *Zeb2*, and *Twist1* expression (as the binary logarithm of the fold change [$\log_2$FC]) in intima samples from *Apoe*$^{-/-}$*Lmna*$^{+/+}$ mice (n=4 or 5, each pool containing RNA from 10–13 animals), *Apoe*$^{-/-}$*Lmna*$^{G609G/G609G}$ mice (n=3, each pool containing RNA from 10–16 animals), *Apoe*$^{-/-}$*Lmna*$^{LCS/LCS}$ mice (n=3, each pool containing RNA from 10 animals), and *Apoe*$^{-/-}$*Lmna*$^{LCS/LCS}$*SM22αCre* mice (n=3, each pool containing RNA from 7 or 8 animals). **C**, Heatmaps showing the expression ($\log_2$FC) of EndMT-linked genes characteristic of endothelial cells (ECs), vascular smooth muscle cells (VSMCs), and fibroblasts in intima samples from *Apoe*$^{-/-}$*Lmna*$^{+/+}$ mice (n=4 or 5, each pool containing RNA from 10–13 animals), *Apoe*$^{-/-}$*Lmna*$^{G609G/G609G}$ mice (n=3, each pool containing RNA from 10–16 animals), *Apoe*$^{-/-}$*Lmna*$^{LCS/LCS}$ mice (n=3, each pool containing RNA from 10 animals), and *Apoe*$^{-/-}$*Lmna*$^{LCS/LCS}$*SM22αCre* mice (n=3, each pool containing RNA from 7 or 8 animals). Data are presented as mean ± SEM together with individual values in **B** and as mean in **C**. Statistical analysis was by 2-tailed *t* test. **P*< 0.05; ***P*< 0.01; ****P*< 0.001; *****P*< 0.0001; ns, not significant.

expression of *Cdh2*, *Mmp2*, *Timp1*, *Fbn1*, and *Comp* in the intima of both progeroid models (Figure 3C). In addition, we detected significant elevation of *Col3a1*, *Col1a1*, and *Col1a2* mRNA in aortic intima of *Apoe*$^{-/-}$*Lmna*$^{LCS/LCS}$*SM22αCre* mice and a trend toward elevation of these mRNAs in *Apoe*$^{-/-}$*Lmna*$^{G609G/G609G}$ mice (Figure 3C). Overall, these quantitative polymerase chain reaction data indicate that ECs in HGPS mouse intima undergo a phenotypic switch to become fibroblast-like cells with high extracellular matrix production. It is interesting that we found increased expression of *Lamb1* in the intima of both models and decreased expression of *Lamb2* in *Apoe*$^{-/-}$*Lmna*$^{LCS/LCS}$*SM22αCre* intima (Figure S15), consistent with laminin β2 to β1 isoform switching linked to EC aging and EndMT.[26] We also detected intimal upregulation in one or both of the progeroid models of *Col8a1* and *Col8a2* (Figure 3C), which encode the atherosclerosis-associated collagen VIII.[27] In general, gene expression changes were more prominent in *Apoe*$^{-/-}$*Lmna*$^{LCS/LCS}$*SM22αCre* mice than in *Apoe*$^{-/-}$*Lmna*$^{G609G/G609G}$ mice, in line with the more advanced vascular disease observed in mice with VSMC-specific progerin expression compared with age-matched mice that express progerin ubiquitously.[15] To provide a more comprehensive view of the processes taking place in the progeroid aortic intima, we performed a high-throughput RNA sequencing analysis in a separate cohort of normal chow–fed 16-week-old mice. These studies confirmed alterations in EndMT-related genes and identified additional alterations in the progeroid aortic intima (Supplemental Results; Figures S16 through S18; Data Sets S5 through S12).

We next validated gene expression changes by immunostaining atheromas from HFD-fed animals for CDH2 (N-cadherin; *Cdh2* gene product), a protein highly expressed in mesenchymal cells and associated with increased migratory and invasive cell behavior.[28] Compared with their respective controls, both *Apoe*$^{-/-}$*Lmna*$^{G609G/G609G}$ and *Apoe*$^{-/-}$*Lmna*$^{LCS/LCS}$*SM22αCre* mice showed enhanced intraplaque CDH2 expression (Figure 4A; Figure S19). Because EndMT affects extracellular matrix production, we next examined atherosclerotic plaques for the expression of collagen IV, which is abundantly produced by ECs, and collagen III, which is produced by fibroblasts and ECs undergoing EndMT.[29] Progeroid mice had elevated intraplaque collagen IV and collagen III expression (Figure 4B and 4C; Figures S20 and S21). It is important to note that CD31-rich atheroma regions also expressed both types of collagens and CDH2 (Figure 4A through 4C), indicating the presence of cells with an intermediate phenotype in progeroid atherosclerotic lesions.

EndMT typically involves enhanced proliferation, and we therefore examined Ki67 expression in neointimal CD31$^+$ cells. The number of Ki67$^+$CD31$^+$ cells per mm^2 in the luminal EC monolayer was not increased in *Apoe*$^{-/-}$*Lmna*$^{G609G/G609G}$ and *Apoe*$^{-/-}$*Lmna*$^{LCS/LCS}$*SM22αCre* mice (Figure 4D); however, both progeroid models had higher counts of Ki67$^+$CD31$^+$ cells per mm^2 inside atheromas (excluding the luminal ECs) (Figure 4D), suggesting that ECs undergoing EndMT proliferate after migrating towards the interior of a lesion. It is interesting that the increase in intraplaque Ki67$^+$CD31$^+$ cell number was more prominent in *Apoe*$^{-/-}$*Lmna*$^{LCS/LCS}$*SM22αCre* mice, which typically have more severe vascular disease than the ubiquitous HGPS model.[15]

Another possible explanation of the abnormal presence of intraplaque CD31$^+$ cells in progeroid aortas is a putative transdifferentiation process whereby progerin-expressing VSMCs lose VSMC markers and upregulate EC markers.[30,31] To investigate this possibility, we traced cells of VSMC origin in the *Apoe*$^{-/-}$*Lmna*$^{LCS/LCS}$*SM22αCre* model through the expression of progerin. If intraplaque CD31$^+$ cells originated from VSMCs, then 100% of these cells would express progerin even if they had lost their VSMC markers, because Cre-mediated excision of the loxP-flanked sequences in the genome of *Apoe*$^{-/-}$*Lmna*$^{LCS/LCS}$*SM22αCre* mice is irreversible (Figure S22A). Immunofluorescence analysis revealed progerin expression in only 34.2% of intraplaque CD31$^+$ cells in *Apoe*$^{-/-}$*Lmna*$^{LCS/LCS}$*SM22αCre* mice (Figure S22B and S22C), indicating that most intraplaque cells with intermediate phenotypes do not derive from transdifferentiated VSMCs.

We next examined specific markers of macrophages (galectin-3; MAC2) and ECs (ERG) by confocal immunofluorescence in *Apoe*$^{-/-}$*Lmna*$^{G609G/G609G}$ and *Apoe*$^{-/-}$*Lmna*$^{LCS/LCS}$*SM22αCre* atheromas. These studies revealed spatial separation of MAC2 and ERG (percentage of MAC2$^+$ cells expressing ERG, 0.2%±0.07% in the ubiquitous model and 0.6%±0.2% in the VSMC-specific model; Figure S23), suggesting that macrophage transdifferentiation to ECs is an unlikely event in the mouse progeroid atherosclerotic aorta.

Transforming Growth Factor β1 Upregulation in Atheromas of Ubiquitous and VSMC-Specific Progeroid Mice

The most common inducer of EndMT is TGF (transforming growth factor) β signaling,[32] which showed profound alterations in the RNA sequencing analysis of the progeroid intima samples (Figures S17B and S24). We therefore investigated the activity of this pathway in progeroid mice by measuring TGFβ1 and TGFβ2 in serum and aorta of 16-week-old mice fed normal chow (Figure 5A). Multiplex assay revealed elevated serum TGFβ2 in *Apoe*$^{-/-}$*Lmna*$^{G609G/G609G}$ mice versus *Apoe*$^{-/-}$*Lmna*$^{+/+}$ controls but no alteration in serum TGFβ1 (Figure 5B). In line with the tissue specificity of the *Apoe*$^{-/-}$*Lmna*$^{LCS/LCS}$*SM22αCre* model, serum TGFβ1 and TGFβ2 were not altered compared

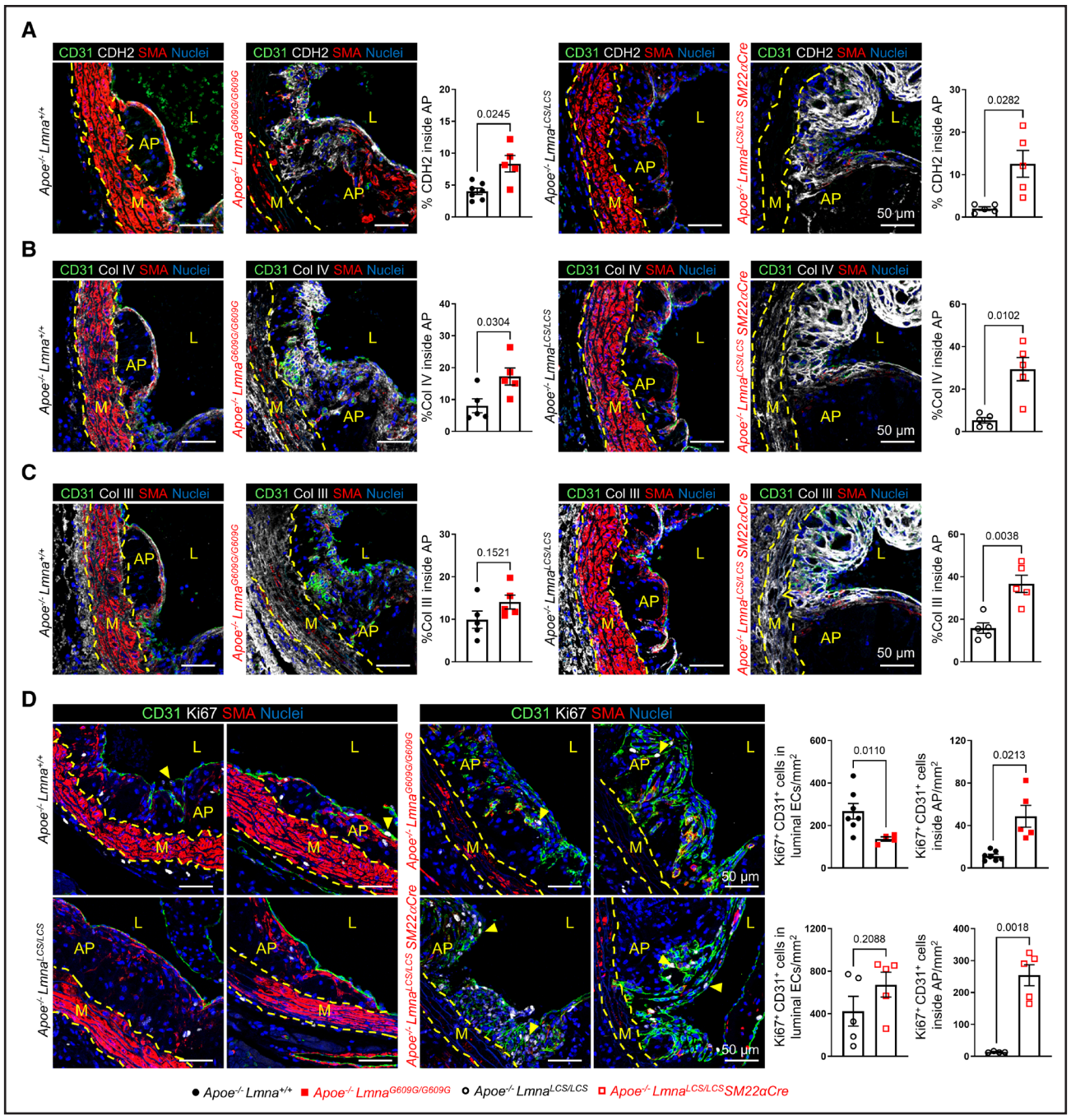

Figure 4. Features of endothelial-to-mesenchymal transition inside atheromas of fat-fed *Apoe*$^{-/-}$*Lmna*$^{G609G/G609G}$ and *Apoe*$^{-/-}$*Lmna*$^{LCS/LCS}$*SM22αCre* mice.

Starting at 8 weeks of age, male mice were fed a high-fat diet for 8 weeks and then euthanized at 16 weeks of age. Serial sections were prepared from paraffin-embedded aortic root samples for immunofluorescence studies. Representative images are shown with nuclei visualized with Hoechst 33342. **A**, CDH2 (N-cadherin), CD31, and SMA (smooth muscle α-actin) expression in atherosclerotic plaques. Graphs show quantification of the CDH2-positive area inside atheromas (excluding necrotic core and luminal endothelial cells [ECs]) in *Apoe*$^{-/-}$*Lmna*$^{+/+}$ (n=7), *Apoe*$^{-/-}$*Lmna*$^{G609G/G609G}$ (n=5), *Apoe*$^{-/-}$*Lmna*$^{LCS/LCS}$ (n=5), and *Apoe*$^{-/-}$*Lmna*$^{LCS/LCS}$*SM22αCre* mice (n=5). **B**, Col IV (collagen IV), CD31, and SMA expression in atherosclerotic plaques. Graphs show quantification of the Col IV–positive area inside atheromas (excluding necrotic core and luminal ECs) in *Apoe*$^{-/-}$*Lmna*$^{+/+}$ mice (n=5), *Apoe*$^{-/-}$*Lmna*$^{G609G/G609G}$ mice (n=5), *Apoe*$^{-/-}$*Lmna*$^{LCS/LCS}$ mice (n=5), and *Apoe*$^{-/-}$*Lmna*$^{LCS/LCS}$*SM22αCre* mice (n=5). **C**, Col III (collagen III), CD31, and SMA expression in atherosclerotic plaques. Graphs show quantification of the Col III–positive area inside atheromas (excluding necrotic core and luminal ECs) in *Apoe*$^{-/-}$*Lmna*$^{+/+}$ mice (n=5), *Apoe*$^{-/-}$*Lmna*$^{G609G/G609G}$ mice (n=5), *Apoe*$^{-/-}$*Lmna*$^{LCS/LCS}$ mice (n=5), and *Apoe*$^{-/-}$*Lmna*$^{LCS/LCS}$*SM22αCre* mice (n=5). **D**, Ki67, CD31, and SMA expression in atherosclerotic plaques. Yellow arrowheads indicate examples of Ki67^{+}CD31^{+} cells. Graphs show the number of Ki67^{+}CD31^{+} cells per mm^2 in the luminal EC monolayer (**left**) and inside atheromas (excluding necrotic core and luminal ECs; **right**) in *Apoe*$^{-/-}$*Lmna*$^{+/+}$ mice (n=7), *Apoe*$^{-/-}$*Lmna*$^{G609G/G609G}$ mice (n=4 or 5), *Apoe*$^{-/-}$*Lmna*$^{LCS/LCS}$ mice (n=4 or 5), and *Apoe*$^{-/-}$*Lmna*$^{LCS/LCS}$*SM22αCre* mice (n=5). Data are presented as mean ± SEM together with individual values. Statistical analysis was by 2-tailed *t* test with Welch correction, and the *P* values are shown. Lower magnification images for **A** through **C** are shown in Figures S19 through S21. Scale bars, 50 μm. AP indicates atherosclerotic plaque; L, lumen; and M, media.

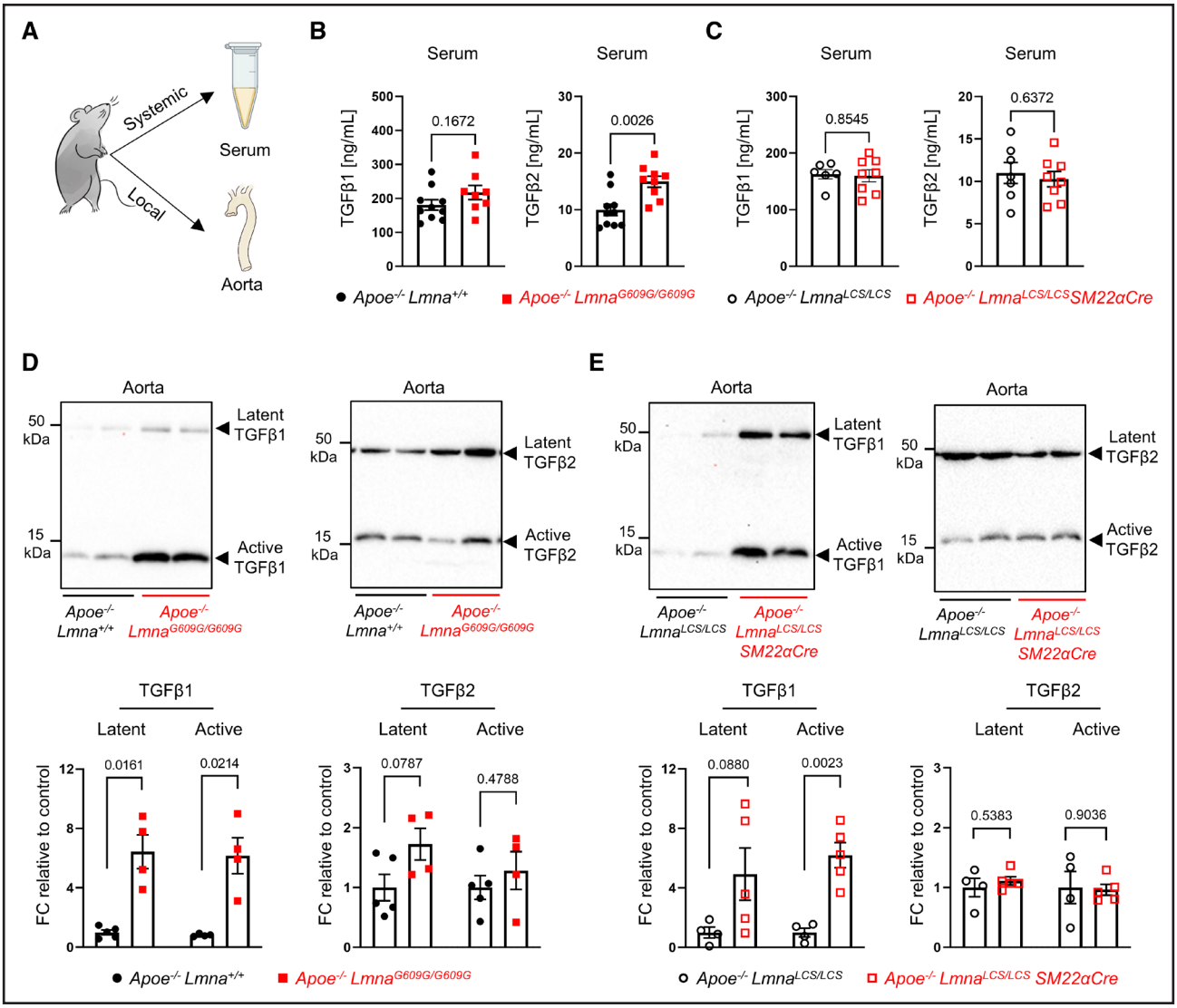

Figure 5. TGF (transforming growth factor) β1 levels are increased in the aorta but not in serum of *Apoe*$^{-/-}$*Lmna*$^{G609G/G609G}$ and *Apoe*$^{-/-}$*Lmna*$^{LCS/LCS}$*SM22αCre* mice.

Male mice fed normal chow were euthanized at 16 weeks of age. **A**, Samples collected for the analysis of the systemic (serum) and local (aorta) levels of TGFβ1 and TGFβ2. **B**, Multiplex assay quantification of TGFβ1 and TGFβ2 in serum of *Apoe*$^{-/-}$*Lmna*$^{+/+}$ mice (n=10) and *Apoe*$^{-/-}$*Lmna*$^{G609G/G609G}$ mice (n=8 or 9). **C**, Multiplex assay quantification of TGFβ1 and TGFβ2 in serum of *Apoe*$^{-/-}$*Lmna*$^{LCS/LCS}$ mice (n=6 or 7) and *Apoe*$^{-/-}$*Lmna*$^{LCS/LCS}$*SM22αCre* mice (n=8). **D**, Representative images of Western blots showing active and latent TGFβ1 and TGFβ2 expression in aorta. Graphs show relative protein levels determined from band densitometry measurements in *Apoe*$^{-/-}$*Lmna*$^{+/+}$ mice (n=4 or 5; pools of 2 or 3 mice) and *Apoe*$^{-/-}$*Lmna*$^{G609G/G609G}$ mice (n=4; pools of 2 or 3 mice). **E**, Representative images of Western blots showing active and latent TGFβ1 and TGFβ2 expression in aorta. Graphs show relative protein levels determined from band densitometry measurements in *Apoe*$^{-/-}$*Lmna*$^{LCS/LCS}$ mice (n=4; pools of 2 or 3 mice) and *Apoe*$^{-/-}$*Lmna*$^{LCS/LCS}$*SM22αCre* mice (n=5; pools of 2 or 3 mice). Total protein assessed by Ponceau S staining was used as a loading control. Ponceau S staining and the uncropped Western blot images are shown in Figure S25. Data are presented as mean ± SEM together with individual values. Statistical analysis was by 2-tailed *t* test in **B** and **C**, and by 2-tailed *t* test with Welch correction in **D** and **E**, and the *P* values are shown.

with *Apoe*$^{-/-}$*Lmna*$^{LCS/LCS}$ control littermates (Figure 5C). Western blot analysis revealed increased expression (≥5-fold) of latent and active forms of TGFβ1, but not TGFβ2, in the aortas of *Apoe*$^{-/-}$*Lmna*$^{G609G/G609G}$ and *Apoe*$^{-/-}$*Lmna*$^{LCS/LCS}$*SM22αCre* mice (Figure 5D and 5E; Figures S25 and S26). Moreover, immunofluorescence analysis showed elevated expression of TGFβ1, but not TGFβ2, in atherosclerotic plaques of HFD-fed 16-week-old mice with ubiquitous and VSMC-specific progerin expression (Figure 6A and 6B). These findings indicate that TGFβ1 is increased locally in the aorta and atheroma in progeroid mice without systemic upregulation. Furthermore, atherosclerotic lesions in both progeroid models had higher numbers of intraplaque CD31^{+} cells expressing the phosphorylated (active) form of SMAD3 (pSMAD3) (Figure 6C), consistent with the activation of the canonical TGFβ pathway in ECs undergoing EndMT in the progeroid aorta. Additional experiments identified

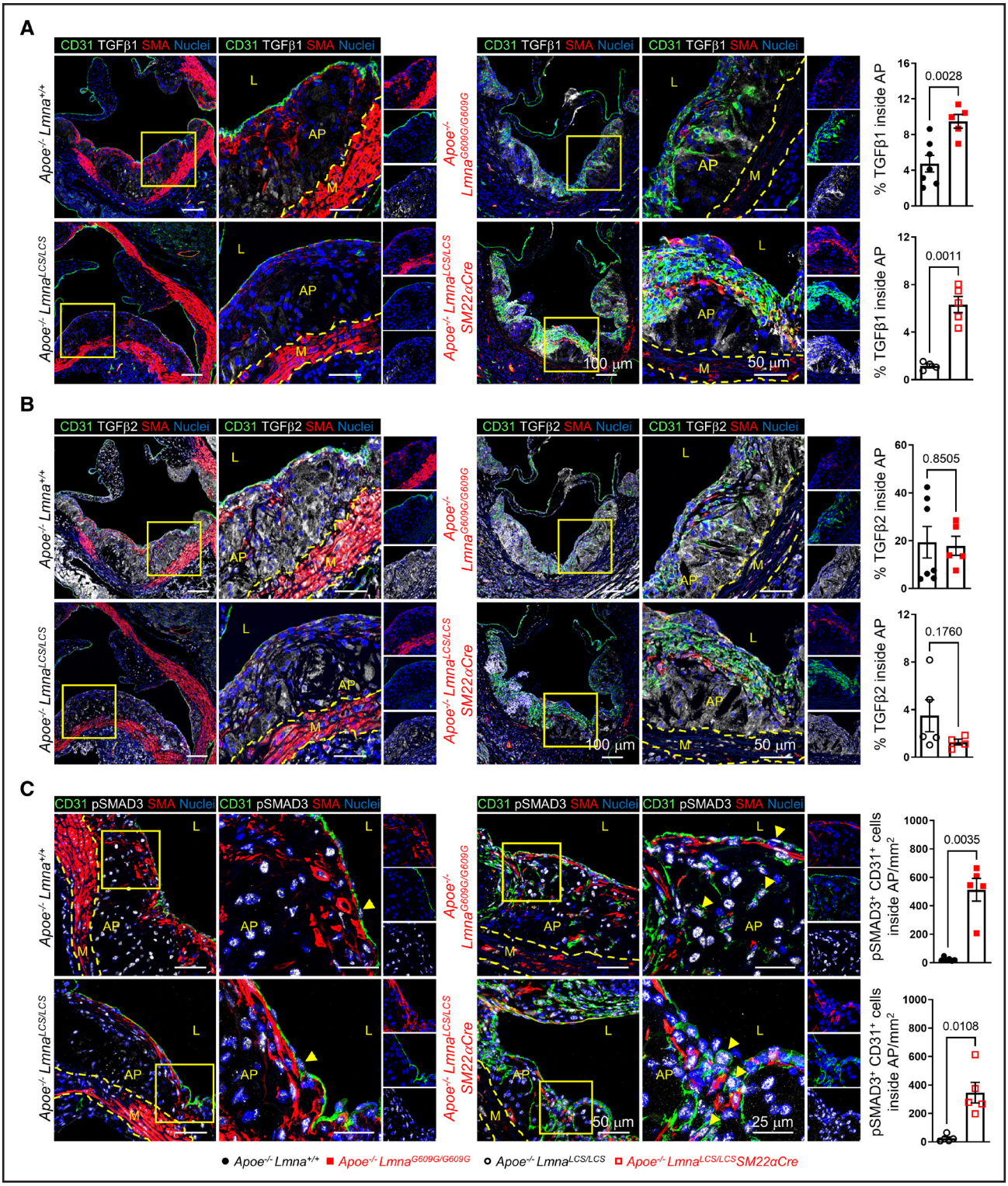

Figure 6. Activation of TGF (transforming growth factor) β1 signaling inside atheromas of fat-fed *Apoe*$^{-/-}$*Lmna*$^{G609G/G609G}$ and *Apoe*$^{-/-}$*Lmna*$^{LCS/LCS}$*SM22αCre* mice.

Starting at 8 weeks of age, male mice were fed a high-fat diet for 8 weeks and euthanized at 16 weeks of age. Serial sections were prepared from paraffin-embedded aortic root samples for immunofluorescence studies. Representative images are shown with nuclei visualized with Hoechst 33342. **A**, TGFβ1, CD31, and SMA (smooth muscle α-actin) expression in atherosclerotic plaques. Scale bar, 100 μm (lower magnification images, **left**), and 50 μm (higher magnification images, **right**). Graphs show quantification of the TGFβ1-positive area inside atheromas (excluding necrotic core and luminal endothelial cells [ECs]) in *Apoe*$^{-/-}$*Lmna*$^{+/+}$ mice (n=7), *Apoe*$^{-/-}$*Lmna*$^{G609G/G609G}$ mice (n=5), *Apoe*$^{-/-}$*Lmna*$^{LCS/LCS}$ mice (n=4), and *Apoe*$^{-/-}$*Lmna*$^{LCS/LCS}$*SM22αCre* mice (n=5). **B**, TGFβ2, CD31, and SMA expression in atherosclerotic plaques. Scale bar, 100 μm (lower magnification images, **left**) and 50 μm (higher magnification images, **right**). Graphs show quantification (*Continued*)

Figure 6 Continued. of the TGFβ2-positive area inside atheromas (excluding necrotic core and luminal ECs) in *Apoe*$^{-/-}$*Lmna*$^{+/+}$ mice (n=7), *Apoe*$^{-/-}$*Lmna*$^{G609G/G609G}$ mice (n=5), *Apoe*$^{-/-}$*Lmna*$^{LCS/LCS}$ mice (n=5), and *Apoe*$^{-/-}$*Lmna*$^{LCS/LCS}$*SM22αCre* mice (n=4). **C**, pSMAD3 (phosphorylated SMAD3), CD31, and SMA expression in atherosclerotic plaques. Scale bar, 50 µm (lower magnification images, **left**) and 25 µm (higher magnification images, **right**). Yellow arrowheads indicate examples of pSMAD3^{+}CD31^{+} cells. Graphs show the number of pSMAD3^{+}CD31^{+} cells per mm^2 inside atheromas (excluding necrotic core and luminal ECs) in *Apoe*$^{-/-}$*Lmna*$^{+/+}$ mice (n=6), *Apoe*$^{-/-}$*Lmna*$^{G609G/G609G}$ mice (n=5), *Apoe*$^{-/-}$*Lmna*$^{LCS/LCS}$ mice (n=5), and *Apoe*$^{-/-}$*Lmna*$^{LCS/LCS}$*SM22αCre* mice (n=5). Data are presented as mean ± SEM together with individual values. Statistical analysis was by 2-tailed *t* test with Welch correction, and the *P* values are shown. AP indicates atherosclerotic plaque; L, lumen; and M, media.

VSMCs and ECs as sources of TGFβ1 upregulation in aortas of ubiquitous and VSMC-specific progeroid mice (Supplemental Results; Figures S27 through S30).

pSMAD3 Inhibition Ameliorates the Progerin-Induced Vascular Phenotype

To explore the therapeutic benefits of inhibiting SMAD3 phosphorylation for progerin-induced vascular disease, we treated mice with SIS3, which reduces TGFβ1-induced SMAD3 phosphorylation and its subsequent interaction with SMAD4 and binding to target DNA sequences.[19] The ability of SIS3 to reduce pSMAD3 levels was assessed in 12-week-old *Apoe*$^{-/-}$*Lmna*$^{LCS/LCS}$*SM22αCre* mice and *Apoe*$^{-/-}$*Lmna*$^{LCS/LCS}$ controls injected with a single dose of the drug (5 µg/g body weight) or vehicle (0.5% dimethyl sulfoxide). Western blot analysis of aortic tissue confirmed pSMAD3 upregulation in vehicle-treated *Apoe*$^{-/-}$*Lmna*$^{LCS/LCS}$*SM22αCre* mice versus *Apoe*$^{-/-}$*Lmna*$^{LCS/LCS}$ controls, and control and progeroid mice both showed reduced pSMAD3 levels 1 and 4 hours after SIS3 inoculation, with the levels beginning to recover 24 hours after SIS3 injection (Figure 7A; Figure S31). We then subjected 8-week-old *Apoe*$^{-/-}$*Lmna*$^{LCS/LCS}$*SM22αCre* mice to a chronic treatment with SIS3 or vehicle for 8 weeks, during which they were fed either normal chow or HFD (Figure 7B). SIS3 treatment did not significantly alter the cholesterol level (Figure S32) or hematological parameters (Figures S33 and S34). However, in *Apoe*$^{-/-}$*Lmna*$^{LCS/LCS}$*SM22αCre* mice fed normal chow, SIS3 therapy significantly reduced leukocyte recruitment to the aortic wall (Figure 7C). Moreover, HFD-fed *Apoe*$^{-/-}$*Lmna*$^{LCS/LCS}$*SM22αCre* mice treated with SIS3 had a slightly milder atherosclerotic plaque burden in the thoracic aorta than vehicle-treated counterparts (Figure 7D), together with significantly elevated medial VSMC content (Figure 7E) and diminished adventitial thickness (Figure 7F), indicating amelioration of progerin-driven vascular disease. SIS3-treated *Apoe*$^{-/-}$*Lmna*$^{LCS/LCS}$*SM22αCre* animals also showed significant reduction in intraplaque collagen IV and collagen III expression (Figure 7G and 7H), consistent with inhibition of EndMT.

DISCUSSION

This study explored the impact of VSMC alterations on ECs in HGPS aorta and its implications for vascular pathology. We found that progerin-driven VSMC defects trigger EC dysfunction and induce EndMT, contributing to atheroma formation. This process is dependent, at least in part, on SMAD3-mediated TGFβ1 signaling, and inhibition of this pathway improved the vascular phenotype of *Apoe*$^{-/-}$*Lmna*$^{LCS/LCS}$*SM22αCre* mice.

Although many studies have investigated HGPS mechanisms since the discovery of the HGPS-causing mutation in 2003,[1,2] very few have focused on atherosclerosis, the death-causing complication in HGPS. We previously reported the first HGPS mouse model showing accelerated atherosclerosis, together with other alterations in the aortic wall characteristic of this syndrome.[15,17,33] Moreover, we have demonstrated that VSMC-specific but not myeloid cell–specific progerin expression is sufficient to provoke VSMC loss, adventitial thickening, accelerated atherogenesis, and premature death in mice.[15] We also found that ubiquitous and VSMC-specific progerin expression both promote a vulnerable plaque phenotype that can result in atheroma disruption and its life-threatening complications, such as myocardial infarction.[15] The importance of VSMCs in progeria was further confirmed by the generation of the progeroid *HGPSrevSM22αCre* mouse model, which expressed progerin throughout the body except for VSMCs and some cardiac cells.[34] Relative to *HGPSrev* mice with ubiquitous progerin expression, *HGPSrevSM22αCre* mice showed substantial amelioration of the vascular phenotype and had a longer lifespan. Furthermore, our previous transcriptomic studies of the VSMC-rich medial aortas of ubiquitous and VSMC-specific HGPS mouse models identified endoplasmic reticulum stress and the unfolded protein response as mechanisms contributing to VSMC death in the artery wall, which in turn accelerates atherogenesis.[35,36] Accordingly, treatment with tauroursodeoxycholic acid to alleviate this stress response partially restored medial and atheroma VSMC content and inhibited atherosclerosis in progeroid mice.[35] Given that *Apoe*$^{-/-}$ mice with progerin expression in VSMCs fully manifest the HGPS-associated vascular phenotype, but not the whole-body phenotype,[15,17] we hypothesized that progerin-driven VSMC alterations and death can orchestrate pathological changes in ECs, whose dysfunction is known to play a major role in atherosclerosis initiation and progression. Our current results in both the ubiquitous and VSMC-specific HGPS models show EC alterations, including increased permeability to LDL, enhanced leukocyte recruitment, and extensive EndMT (Figure 8).

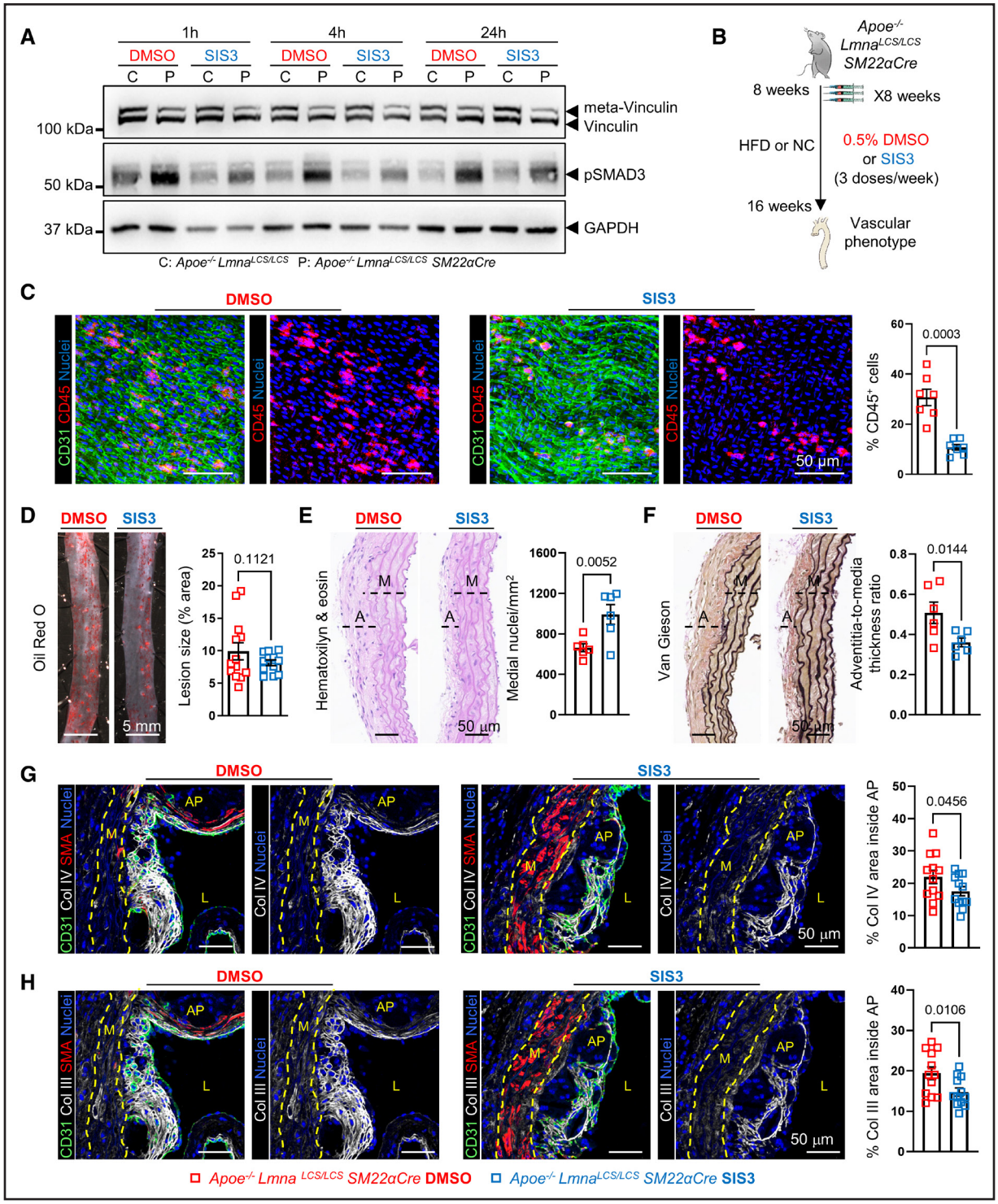

Figure 7. Inhibition of SMAD3 phosphorylation with SIS3 (specific inhibitor of SMAD3) ameliorates vascular alterations in *Apoe*$^{-/-}$*Lmna*$^{LCS/LCS}$*SM22αCre* mice.

A, Western blot analysis of pSMAD3 (phosphorylated SMAD3), vinculin, and GAPDH in aortas of *Apoe*$^{-/-}$*Lmna*$^{LCS/LCS}$ (C, control) and *Apoe*$^{-/-}$*Lmna*$^{LCS/LCS}$*SM22αCre* (P, progeroid) mice 1, 4, and 24 hours after receiving a single injection of the specific SMAD3 inhibitor SIS3 or vehicle (0.5% dimethyl sulfoxide [DMSO]). Each lane corresponds to a pool of 2 aortas of the same genotype and treatment. The experiment was performed in 12-week-old male mice fed normal chow (NC). Ponceau S staining and the uncropped Western blot images are shown in Figure S31. **B**, Experimental design for the in vivo assessment of the therapeutic effects of chronic SIS3 treatment. Starting at 8 weeks of age, *Apoe*$^{-/-}$*Lmna*$^{LCS/LCS}$*SM22αCre* male mice were treated with either SIS3 or 0.5% DMSO 3 times a week for 8 weeks. Animals were fed during treatment with NC or a high-fat diet (HFD) (**D** through **H**) and euthanized at 16 weeks of age. **C**, Representative immunofluorescence images showing CD45 and CD31 expression in en face aorta preparations. Hoechst 33342 was used to visualize nuclei. Scale bar, 50 μm. The graph shows leukocyte recruitment quantified as the percentage of CD45-positive nuclei in aortas of SIS3- or (*Continued*)

Figure 7 Continued. vehicle-treated *Apoe*$^{-/-}$*Lmna*$^{LCS/LCS}$*SM22αCre* mice (n=7 per group). **D**, Representative en face images of thoracic aorta stained with Oil Red O (ORO; red). Scale bar, 5 mm. The graph shows atherosclerosis burden quantified as the percentage of ORO-stained aortic surface in SIS3- or vehicle-treated *Apoe*$^{-/-}$*Lmna*$^{LCS/LCS}$*SM22αCre* mice (n=12 or 13 per group). **E**, Representative images of thoracic aorta cross-sections stained with hematoxylin and eosin. Scale bar, 50 µm. The graph shows quantification of nuclei number per mm^2 in the medial layer of SIS3-treated or vehicle-treated *Apoe*$^{-/-}$*Lmna*$^{LCS/LCS}$*SM22αCre* mice (n=6 per group). **F**, Representative images of thoracic aorta cross-sections stained with van Gieson stain. Scale bar, 50 µm. The graph shows the adventitia-to-media thickness ratio in SIS3-treated or vehicle-treated *Apoe*$^{-/-}$*Lmna*$^{LCS/LCS}$*SM22αCre* mice (n=6 per group). **G** and **H**, Representative immunofluorescence images showing CD31, SMA (smooth muscle α-actin) and Col IV (collagen IV) (**G**) or Col III (collagen III) (**H**) expression in atherosclerotic plaques in the aortic root. Hoechst 33342 was used to visualize nuclei. Scale bar, 50 µm. Graphs show quantification of the percentage Col IV–positive or Col III–positive area inside atheromas (excluding necrotic core and luminal ECs) in SIS3-treated or vehicle-treated *Apoe*$^{-/-}$*Lmna*$^{LCS/LCS}$*SM22αCre* mice (n=12 per group). Data are presented as mean ± SEM together with individual values. Statistical analysis was by 1-tailed *t* test with Welch correction in **C** and **D** and by 1-tailed *t* test in **E** through **H**, and the *P* values are shown. A indicates adventitia; AP, atherosclerotic plaque; L, lumen; and M, media.

The aortas of *Apoe*-deficient mice with ubiquitous or VSMC-specific progerin expression show increased accumulation of lipids in the medial layer, and in vivo experiments with fluorescently labeled human LDL revealed that this excessive lipid content is associated with increased LDL retention.[15] Using the same experimental approach, we show here that lipid accumulation in the arterial wall of HGPS mice is also mediated by increased endothelial permeability to LDL. Augmented LDL permeability and retention could explain the early onset of atherosclerosis in patients with HGPS typically in the absence of hypercholesterolemia.[37] Moreover, progerin expression in both models increased the numbers of leukocytes adhering to or migrating through the aortic endothelium, likely contributing to neointimal growth.

Our study also identifies EndMT as another important characteristic of progeroid ECs, which acquire features of mesenchymal cells (see also "Transcriptomic Alterations in the Intima of the Ubiquitous and VSMC-Specific Progeria Models" in Supplemental Discussion). It is important to note that EndMT has been linked to many pathological processes, including atherosclerosis.[38] Analysis of progerin expression in CD31-positive cells in *Apoe*$^{-/-}$*Lmna*$^{LCS/LCS}$*SM22αCre* mice indicated that most intraplaque CD31$^+$ cells with an intermediate phenotype do not originate from transdifferentiated VSMCs. Given that SM22α can be induced during EndMT towards VSMCs or myofibroblasts, the presence of a fraction of progerin-expressing CD31$^+$ cells in atheroma plaques of *Apoe*$^{-/-}$*Lmna*$^{LCS/LCS}$*SM22αCre* mice is consistent with EndMT as the origin of intraplaque CD31$^+$ cells of intermediate phenotype. Macrophages seem not to be the source of an EC-like population inside progeroid atheromas, because no substantial colocalization of endothelial and macrophage markers was found in *Apoe*$^{-/-}$*Lmna*$^{G609G/G609G}$ or *Apoe*$^{-/-}$*Lmna*$^{LCS/LCS}$*SM22αCre* mice. Nonetheless, future linage tracing experiments are warranted to confirm ECs as the main source of the intraplaque CD31/ERG/VWF-positive population.

EndMT in HGPS atherosclerotic plaques seems to be partial, with many cells retaining EC markers although they have lost cell polarity and express mesenchymal markers. This may reflect a general tendency for postnatal EndMT to be incomplete[39,40]; nevertheless, it is also possible that intraplaque ECs in progeroid mice are restrained from a more complete mesenchymal transition by the reduced expression of *Twist1* and *Snai2*. Analyses of gene expression profiles in the intima and protein expression in the atherosclerotic lesions indicate that ECs in HGPS plaques acquire characteristics of fibroblast-like cells that produce substantial amounts of extracellular matrix–related proteins, and that this process seems to be mediated by upregulation of *Snai1*. Given our previous identification of chondrocyte-like cells in atheroma lesions of aged *Apoe*$^{-/-}$*Lmna*$^{LCS/LCS}$*SM22αCre* mice,[15] we propose that EndMT can give rise to a variety of cell types in atherosclerotic lesions during HGPS progression. Further studies are required to assess whether EndMT might contribute to pathological changes in other HGPS tissues and organs.

EndMT in the ubiquitous and VSMC-specific progeria models seems to be triggered, at least partially, by SMAD3-mediated TGFβ1 signaling. Both models showed increased TGFβ1 content in the aorta and atheromas while maintaining normal serum TGFβ1 concentration. Moreover, treatment of *Apoe*$^{-/-}$*Lmna*$^{LCS/LCS}$*SM22αCre* mice with SIS3 inhibited SMAD3 phosphorylation in the aorta and triggered improvements in the progerin-induced phenotype, including a tendency towards reduction of atherosclerosis burden and significant reductions in adventitial thickening, medial VSMC loss, and leukocyte recruitment. SIS3 is highly selective for SMAD3 and has no effect on SMAD2 phosphorylation, the protein expression of SMAD4 and SMAD7, or the phosphorylation of effectors of other signaling pathways.[19] Nonetheless, the relatively moderate inhibitory effect of SIS3 on atherosclerosis in *Apoe*$^{-/-}$*Lmna*$^{LCS/LCS}$*SM22αCre* mice could be related to its limited bioavailability in vivo, given its low aqueous solubility. Further studies are warranted to assess the therapeutic benefits on atherosclerosis of a more water-soluble SIS3 analogue[41] or the recently reported self-carried nanodrug-SIS3.[42] It is also important to note that EndMT can be induced by processes other than TGFβ1/SMAD3 signaling, including oscillatory- and low-shear stress,[43–45] oxidized LDL actions,[46] NOTCH (notch receptor) signaling,[47] Wnt/β-catenin signaling,[48] oxidative stress,[49]

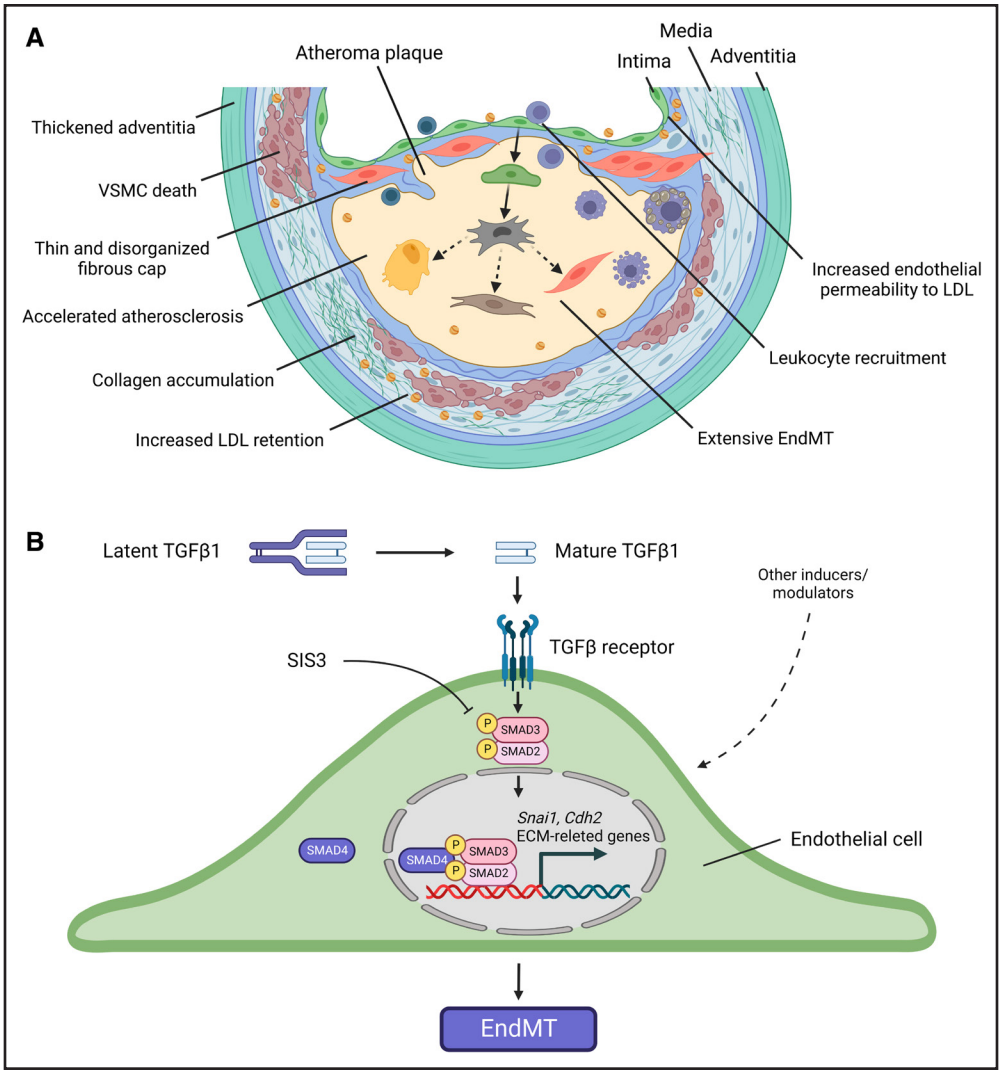

Figure 8. Atherosclerosis in progeria features extensive endothelial-to-mesenchymal transition (EndMT) caused by vascular smooth muscle cell (VSMC) dysfunction and SMAD3-dependent TGF (transforming growth factor) β1 signaling.
A, Main features of vascular disease in mouse models of Hutchinson-Gilford progeria syndrome (HGPS). Both ubiquitous and VSMC-specific progerin expression cause a series of alterations in the medial layer of the arteries, including VSMC loss, collagen accumulation, and excessive low-density lipoprotein (LDL) retention, accompanied by adventitial thickening and inflammation. The intima also shows increased permeability to LDL particles and augmented leukocyte recruitment. These changes in progeroid arteries are associated with accelerated formation of atherosclerotic plaques, which are characterized by a thin or disorganized fibrous cap and extensive EndMT. **B**, Proposed model of EndMT induction during atherosclerosis in progeria. TGFβ1 present in progeroid atheromas triggers phosphorylation of SMAD3 in endothelial cells, which in turn induces the EndMT-related transcriptional program. Nevertheless, additional EndMT inducers/modulators are expected to play a role in this process. Illustrations were created with BioRender.com. ECM indicates extracellular matix; and SIS3, specific inhibitor of SMAD3.

and inflammation.[50] Some of these mechanisms and pathways have been linked to HGPS in cell and mouse models, and it is therefore likely that complementary mechanisms regulate progeria-associated EndMT and that these alternative pathways might partially compensate for TGFβ-signaling inhibition with SIS3. RNA sequencing data from the intima of *Apoe*$^{-/-}$*Lmna*$^{G609G/G609G}$ and *Apoe*$^{-/-}$*Lmna*$^{LCS/LCS}$*SM22αCre* mice further support the notion that other mechanisms alongside TGFβ1/SMAD3 signaling may contribute to or modulate EndMT in progeroid plaques (see "Transcriptomic Alterations in the Intima of the Ubiquitous and VSMC-Specific Progeria Models" in Supplemental Discussion).

The analysis of *Apoe*$^{-/-}$*Lmna*$^{LCS/LCS}$*Cdh5Cre*^{ERT2} and *Apoe*$^{-/-}$*Lmna*$^{LCS/LCS}$*LysMCre* mice indicates that progerin expression in ECs or myeloid cells (including macrophages) is not sufficient to trigger EndMT in atherosclerotic lesions. The examination of *Apoe*$^{-/-}$*Lmna*$^{LCS/LCS}$ *SM22αCre* mice implies that EndMT in HGPS is induced, either directly or indirectly, by dysfunctional or dying VSMCs. Indeed, EndMT in atherosclerotic plaques might be a compensatory process to replenish the diminished population of VSMCs, which typically increase plaque stability by forming a fibrous cap that protects against atherothrombosis. Supporting this idea, Newman and colleagues recently showed that depletion of cells positive

for PDGFRβ (platelet derived growth factor receptor β) in the fibrous cap triggers EndMT to maintain plaque stability.[12] However, in the long run, these EC-derived cells are not equivalent to VSMCs, and lead to plaque instability at later stages of atherosclerosis. These findings are in line with our previous observations that atheromas in the ubiquitous and VSMC-specific HGPS mouse models show signs of plaque disruption, such as the presence of erythrocytes and iron deposits, in some cases leading to myocardial infarction.[15,16] It is important to note that a link between EndMT and vulnerable plaque features has been reported in human atherosclerosis,[38] suggesting that findings in HGPS may be relevant to atherosclerosis during physiological aging (see "Similarities and Differences Between HGPS and Non-HGPS Atherosclerosis" in Supplemental Discussion). Given the recent description of sex differences in EndMT,[51] it would be interesting to address this aspect in future studies of HGPS.

The results of the present study, together with our previous work, indicate that one of the earliest effects of progerin expression in the arterial wall is to induce changes in the phenotype of VSMCs, leading to their dysfunction and death in the arterial media and in the fibrous cap of the atheroma plaque (Figure 8A). This process in turn elicits changes in ECs, including augmented permeability to LDL, immune cell recruitment, and EndMT. As a result, the progeroid atheroma plaque is characterized by the presence of endothelial-like cells with fibroproliferative properties that alter plaque characteristics and likely contribute to plaque instability and rupture. This phenotypic change in ECs appears to be partially dependent on TGFβ1/SMAD3 signaling (Figure 8B), because its inhibition with SIS3 ameliorates vascular alterations in *Apoe*$^{-/-}$*Lmna*$^{LCS/LCS}$*SM22αCre* mice. Nevertheless, other EndMT inducers/modulators (eg, proinflammatory cytokines) are expected to play a role in this process, and further studies are warranted to completely fathom out this intricate event. In summary, our findings identify a novel mechanism involved in premature vascular disease in progeria and offer a new therapeutic target. In addition, these results might help to unravel the complex role of EndMT in atherosclerosis associated with physiological aging.

ARTICLE INFORMATION

Received May 29, 2023; accepted July 26, 2024.

Affiliations

Departamento de Bioquímica y Biología Molecular, Instituto Universitario de Oncología, Universidad de Oviedo, Spain (M.R.H., V.Q., C.L.-O.). Centro de Investigación Biomédica en Red de Enfermedades Cardiovasculares, Spain (M.R.H., R.M.N., P.G., M.J.A.-M., A.D., V.A.). Centro Nacional de Investigaciones Cardiovasculares, Madrid, Spain (R.M.N., P.G., M.J.A.-M., P.N., A.R., C.T., F.S.-C., A.D., J.F.B., V.A.). Centro de Investigación Biomédica en Red de Cáncer, Spain (V.Q.). Department of Clinical Medicine, Aarhus University, Denmark (J.F.B.). Facultad de Ciencias de la Vida y la Naturaleza, Universidad Nebrija, Madrid, Spain (C.L.-O.). Centre de Recherche des Cordeliers, Université de Paris Cité, Sorbonne Université, INSERM U1138, France (C.L.-O.).

Acknowledgments

The authors thank Anna de Andrés for artwork; Simon Bartlett for English editing; Verónica Labrador, Hélio Roque, and Elvira Arza for help with ImageJ macro development; and Eva Santos and the CNIC Animal Facility for animal care. Illustrations were created using BioRender.com (licensed to V.A.).

Sources of Funding

V.A.'s laboratory is supported by grant PID2022-141211OB-I00 funded by Ministerio de Ciencia, Innovación y Universidades (MICIU)/AEI/10.13039/501100011033 and European Regional Development Fund/European Union, and a donation from Asociación Progeria Alexandra Peraut. The CNIC is supported by the Instituto de Salud Carlos III, the MICIU, and the Pro-CNIC Foundation and is a Severo Ochoa Center of Excellence (grant CEX2020-001041-S funded by MICIU/AEI/10.13039/501100011033). Microscopy was conducted at the CNIC Microscopy & Dynamic Imaging ICTS (Unique Science and Technology Infrastructure)–ReDib funded by MICIU/AEI/10.13039/501100011033 and European Regional Development Fund–A Way to Make Europe. Work in the C.L.-O. laboratory is supported by MICIU/AEI/10.13039/501100011033 (grant PDI2020-118394RB-100) and the European Research Council under the European Union's Horizon 2020 research and innovation program (grant agreement No. 742067). R.M.N. was supported by the Ministerio de Educación, Cultura y Deporte (predoctoral contract FPU16/05027). M.R.H. was supported by the MICIU (postdoctoral contract IJC2019-040798-I).

Disclosures

The authors report no conflicts. The funders had no role in the design of the study, the collection, analysis, or interpretation of data, and the reporting of the study.

Supplemental Material

Supplemental Methods
Supplemental Results
Supplemental Discussion
Tables S1–S9
Figures S1–S34
Legends for Supplemental Videos
Titles for Supplemental Data Sets
Videos S1–S12
Data Sets S1–S12
Uncropped Gel Blots
References 52–67

REFERENCES

1. De Sandre-Giovannoli A, Bernard R, Cau P, Navarro C, Amiel J, Boccaccio I, Lyonnet S, Stewart CL, Munnich A, Le Merrer M, et al. Lamin A truncation in Hutchinson-Gilford progeria. *Science*. 2003;300:2055. doi: 10.1126/science.1084125
2. Eriksson M, Brown WT, Gordon LB, Glynn MW, Singer J, Scott L, Erdos MR, Robbins CM, Moses TY, Berglund P, et al. Recurrent de novo point mutations in lamin A cause Hutchinson–Gilford progeria syndrome. *Nature*. 2003;423:293–298. doi: 10.1038/nature01629
3. Dorado B, Andrés V. A-type lamins and cardiovascular disease in premature aging syndromes. *Curr Opin Cell Biol*. 2017;46:17–25. doi: 10.1016/j.ceb.2016.12.005
4. Ullrich NJ, Gordon LB. Hutchinson–Gilford progeria syndrome. *Handb Clin Neurol*. 2015;132:249–264. doi: 10.1016/B978-0-444-62702-5.00018-4
5. Stehbens WE, Wakefield SJ, Gilbert-Barness E, Olson RE, Ackerman J. Histological and ultrastructural features of atherosclerosis in progeria. *Cardiovasc Pathol*. 1999;8:29–39. doi: 10.1016/s1054-8807(98)00023-4
6. Stehbens WE, Delahunt B, Shozawa T, Gilbert-Barness E. Smooth muscle cell depletion and collagen types in progeric arteries. *Cardiovasc Pathol*. 2001;10:133–136. doi: 10.1016/s1054-8807(01)00069-2
7. Olive M, Harten I, Mitchell R, Beers JK, Djabali K, Cao K, Erdos MR, Blair C, Funke B, Smoot L, et al. Cardiovascular pathology in Hutchinson-Gilford progeria: correlation with the vascular pathology of aging. *Arterioscler Thromb Vasc Biol*. 2010;30:2301–2309. doi: 10.1161/ATVBAHA.110.209460
8. Hamczyk MR, Nevado RM, Barettino A, Fuster V, Andrés V. Biological versus chronological aging: JACC Focus Seminar. *J Am Coll Cardiol*. 2020;75:919–930. doi: 10.1016/j.jacc.2019.11.062
9. Basatemur GL, Jørgensen HF, Clarke MCH, Bennett MR, Mallat Z. Vascular smooth muscle cells in atherosclerosis. *Nat Rev Cardiol*. 2019;16:727–744. doi: 10.1038/s41569-019-0227-9

10. van Kuijk K, Kuppe C, Betsholtz C, Vanlandewijck M, Kramann R, Sluimer JC. Heterogeneity and plasticity in healthy and atherosclerotic vasculature explored by single-cell sequencing. *Cardiovasc Res*. 2019;115:1705–1715. doi: 10.1093/cvr/cvz185
11. Kovacic JC, Dimmeler S, Harvey RP, Finkel T, Aikawa E, Krenning G, Baker AH. Endothelial to mesenchymal transition in cardiovascular disease: JACC State-of-the-Art Review. *J Am Coll Cardiol*. 2019;73:190–209. doi: 10.1016/j.jacc.2018.09.089
12. Newman AAC, Serbulea V, Baylis RA, Shankman LS, Bradley X, Alencar GF, Owsiany K, Deaton RA, Karnewar S, Shamsuzzaman S, et al. Multiple cell types contribute to the atherosclerotic lesion fibrous cap by PDGFRβ and bioenergetic mechanisms. *Nat Metab*. 2021;3:166–181. doi: 10.1038/s42255-020-00338-8
13. Méndez-Barbero N, Gutiérrez-Muñoz C, Blanco-Colio LM. Cellular crosstalk between endothelial and smooth muscle cells in vascular wall remodeling. *Int J Mol Sci* . 2021;22:7284. doi: 10.3390/ijms22147284
14. Yurdagul A Jr. Crosstalk between macrophages and vascular smooth muscle cells in atherosclerotic plaque stability. *Arterioscler Thromb Vasc Biol*. 2022;42:372–380. doi: 10.1161/ATVBAHA.121.316233
15. Hamczyk MR, Villa-Bellosta R, Gonzalo P, Andrés-Manzano MJ, Nogales P, Bentzon JF, López-Otín C, Andrés V. Vascular smooth muscle–specific progerin expression accelerates atherosclerosis and death in a mouse model of Hutchinson-Gilford progeria syndrome. *Circulation*. 2018;138:266–282. doi: 10.1161/CIRCULATIONAHA.117.030856
16. Nevado RM, Hamczyk MR, Gonzalo P, Andrés-Manzano MJ, Andrés V. Premature vascular aging with features of plaque vulnerability in an atheroprone mouse model of Hutchinson–Gilford progeria syndrome with Ldlr deficiency. *Cells*. 2020;9:2252. doi: 10.3390/cells9102252
17. Hamczyk MR, Andrés V. Vascular smooth muscle cell loss underpins the accelerated atherosclerosis in Hutchinson-Gilford progeria syndrome. *Nucleus*. 2019;10:28–34. doi: 10.1080/19491034.2019.1589359
18. Percie du Sert N, Hurst V, Ahluwalia A, Alam S, Avey MT, Baker M, Browne WJ, Clark A, Cuthill IC, Dirnagl U, et al. The ARRIVE guidelines 2.0: updated guidelines for reporting animal research. *PLoS Biol*. 2020;18:e3000410. doi: 10.1371/journal.pbio.3000410
19. Jinnin M, Ihn H, Tamaki K. Characterization of SIS3, a novel specific inhibitor of Smad3, and its effect on transforming growth factor-β1-induced extracellular matrix expression. *Mol Pharmacol*. 2006;69:597–607. doi: 10.1124/mol.105.017483
20. Steffensen LB, Mortensen MB, Kjolby M, Hagensen MK, Oxvig C, Bentzon JF. Disturbed laminar blood flow vastly augments lipoprotein retention in the artery wall: a key mechanism distinguishing susceptible from resistant sites. *Arterioscler Thromb Vasc Biol*. 2015;35:1928–1935. doi: 10.1161/ATVBAHA.115.305874
21. Nevado RM, Hamczyk MR, Andrés V. Isolation of mouse aortic RNA for transcriptomics. *Methods Mol Biol*. 2022;2419:611–627. doi: 10.1007/978-1-0716-1924-7_38
22. Lertkiatmongkol P, Liao D, Mei H, Hu Y, Newman PJ. Endothelial functions of platelet/endothelial cell adhesion molecule-1 (CD31). *Curr Opin Hematol*. 2016;23:253–259. doi: 10.1097/MOH.0000000000000239
23. Nikolova-Krstevski V, Yuan L, Le Bras A, Vijayaraj P, Kondo M, Gebauer I, Bhasin M, Carman CV, Oettgen P. ERG is required for the differentiation of embryonic stem cells along the endothelial lineage. *BMC Dev Biol*. 2009;9:72. doi: 10.1186/1471-213X-9-72
24. Al Barashdi MA, Ali A, McMullin MF, Mills K. Protein tyrosine phosphatase receptor type C (PTPRC or CD45). *J Clin Pathol*. 2021;74:548–552. doi: 10.1136/jclinpath-2020-206927
25. Weinstein N, Mendoza L, Álvarez-Buylla ER. A computational model of the endothelial to mesenchymal transition. *Front Genet*. 2020;11:40. doi: 10.3389/fgene.2020.00040
26. Wagner JUG, Chavakis E, Rogg EM, Muhly-Reinholz M, Glaser SF, Günther S, John D, Bonini F, Zeiher AM, Schaefer L, et al. Switch in laminin β2 to laminin β1 isoforms during aging controls endothelial cell functions-brief report. *Arterioscler Thromb Vasc Biol*. 2018;38:1170–1177. doi: 10.1161/ATVBAHA.117.310685
27. Lopes J, Adiguzel E, Gu S, Liu SL, Hou G, Heximer S, Assoian RK, Bendeck MP. Type VIII collagen mediates vessel wall remodeling after arterial injury and fibrous cap formation in atherosclerosis. *Am J Pathol*. 2013;182:2241–2253. doi: 10.1016/j.ajpath.2013.02.011
28. Radice GL. N-cadherin-mediated adhesion and signaling from development to disease: lessons from mice. *Prog Mol Biol Transl Sci*. 2013;116:263–289. doi: 10.1016/B978-0-12-394311-8.00012-1
29. Medici D, Kalluri R. Endothelial–mesenchymal transition and its contribution to the emergence of stem cell phenotype. *Semin Cancer Biol*. 2012;22:379–384. doi: 10.1016/j.semcancer.2012.04.004
30. Wang H, Yan S, Chai H, Riha GM, Li M, Yao Q, Chen C. Shear stress induces endothelial transdifferentiation from mouse smooth muscle cells. *Biochem Biophys Res Commun*. 2006;346:860–865. doi: 10.1016/j.bbrc.2006.05.196
31. Hong X, Margariti A, Le Bras A, Jacquet L, Kong W, Hu Y, Xu Q. Transdifferentiated human vascular smooth muscle cells are a new potential cell source for endothelial regeneration. *Sci Rep*. 2017;7:5590. doi: 10.1038/s41598-017-05665-7
32. Ma J, Sanchez-Duffhues G, Goumans MJ, ten Dijke P. TGF-β-induced endothelial to mesenchymal transition in disease and tissue engineering. *Front Cell Dev Biol*. 2020;8:260. doi: 10.3389/fcell.2020.00260
33. Hamczyk MR, Andrés V. Accelerated atherosclerosis in HGPS. *Aging (Albany NY)*. 2018;10:2555–2556. doi: 10.18632/aging.101608
34. Sánchez-López A, Espinós-Estévez C, González-Gómez C, Gonzalo P, Andrés-Manzano MJ, Fanjul V, Riquelme-Borja R, Hamczyk MR, Macías A, del Campo L, et al. Cardiovascular progerin suppression and lamin A restoration rescue Hutchinson-Gilford progeria syndrome. *Circulation*. 2021;144:1777–1794. doi: 10.1161/CIRCULATIONAHA.121.055313
35. Hamczyk MR, Villa-Bellosta R, Quesada V, Gonzalo P, Vidak S, Nevado RM, Andrés-Manzano MJ, Misteli T, López-Otín C, Andrés V. Progerin accelerates atherosclerosis by inducing endoplasmic reticulum stress in vascular smooth muscle cells. *EMBO Mol Med*. 2019;11:e9736. doi: 10.15252/emmm.201809736
36. Di Pasquale E, Condorelli G. Endoplasmic reticulum stress at the crossroads of progeria and atherosclerosis. *EMBO Mol Med*. 2019;11:e10360. doi: 10.15252/emmm.201910360
37. Gordon LB, Harten IA, Patti ME, Lichtenstein AH. Reduced adiponectin and HDL cholesterol without elevated C-reactive protein: clues to the biology of premature atherosclerosis in Hutchinson-Gilford progeria syndrome. *J Pediatr*. 2005;146:336–341. doi: 10.1016/j.jpeds.2004.10.064
38. Evrard SM, Lecce L, Michelis KC, Nomura-Kitabayashi A, Pandey G, Purushothaman K-R, D'Escamard V, Li JR, Hadri L, Fujitani K, et al. Endothelial to mesenchymal transition is common in atherosclerotic lesions and is associated with plaque instability. *Nat Commun*. 2016;7:11853. doi: 10.1038/ncomms11853
39. Welch-Reardon KM, Wu N, Hughes CCW. A role for partial endothelial-mesenchymal transitions in angiogenesis? *Arterioscler Thromb Vasc Biol*. 2015;35:303–308. doi: 10.1161/ATVBAHA.114.303220
40. Piera-Velazquez S, Jimenez SA. Endothelial to mesenchymal transition: role in physiology and in the pathogenesis of human diseases. *Physiol Rev*. 2019;99:1281–1324. doi: 10.1152/physrev.00021.2018
41. Wu N, Lian G, Sheng J, Wu D, Yu X, Lan H, Hu W, Yang Z. Discovery of a novel selective water-soluble SMAD3 inhibitor as an antitumor agent. *Bioorg Med Chem Lett*. 2020;30:127396. doi: 10.1016/j.bmcl.2020.127396
42. Lian G-Y, Wan Y, Mak TS-K, Wang Q-M, Zhang J, Chen J, Wang Z-Y, Li M, Tang PM-K, Huang X-R, et al. Self-carried nanodrug (SCND-SIS3): a targeted therapy for lung cancer with superior biocompatibility and immune boosting effects. *Biomaterials*. 2022;288:121730. doi: 10.1016/j.biomaterials.2022.121730
43. Kouzbari K, Hossan MR, Arrizabalaga JH, Varshney R, Simmons AD, Gostynska S, Nollert MU, Ahamed J. Oscillatory shear potentiates latent TGF-β1 activation more than steady shear as demonstrated by a novel force generator. *Sci Rep*. 2019;9:6065. doi: 10.1038/s41598-019-42302-x
44. Mahmoud MM, Serbanovic-Canic J, Feng S, Souilhol C, Xing R, Hsiao S, Mammoto A, Chen J, Ariaans M, Francis SE, et al. Shear stress induces endothelial-to-mesenchymal transition via the transcription factor Snail. *Sci Rep*. 2017;7:3375. doi: 10.1038/s41598-017-03532-z
45. Moonen JRAJ, Lee ES, Schmidt M, Maleszewska M, Koerts JA, Brouwer LA, Van Kooten TG, Van Luyn MJA, Zeebregts CJ, Krenning G, et al. Endothelial-to-mesenchymal transition contributes to fibro-proliferative vascular disease and is modulated by fluid shear stress. *Cardiovasc Res*. 2015;108:377–386. doi: 10.1093/cvr/cvv175
46. Su Q, Sun Y, Ye Z, Yang H, Li L. Oxidized low density lipoprotein induces endothelial-to-mesenchymal transition by stabilizing Snail in human aortic endothelial cells. *Biomed Pharmacother*. 2018;106:1720–1726. doi: 10.1016/j.biopha.2018.07.122
47. Chang ACY, Fu Y, Garside VC, Niessen K, Chang L, Fuller M, Setiadi A, Smrz J, Kyle A, Minchinton A, et al. Notch initiates the endothelial-to-mesenchymal transition in the atrioventricular canal through autocrine activation of soluble guanylyl cyclase. *Dev Cell*. 2011;21:288–300. doi: 10.1016/j.devcel.2011.06.022
48. Liebner S, Cattelino A, Gallini R, Rudini N, Iurlaro M, Piccolo S, Dejana E. β-Catenin is required for endothelial-mesenchymal transformation during heart cushion development in the mouse. *J Cell Biol*. 2004;166:359–367. doi: 10.1083/jcb.200403050

49. Montorfano I, Becerra A, Cerro R, Echeverría C, Sáez E, Morales MG, Fernández R, Cabello-Verrugio C, Simon F. Oxidative stress mediates the conversion of endothelial cells into myofibroblasts via a TGF-β1 and TGF-β2-dependent pathway. *Lab Invest*. 2014;94:1068–1082. doi: 10.1038/labinvest.2014.100
50. Sánchez-Duffhues G, García de Vinuesa A, van de Pol V, Geerts ME, de Vries MR, Janson SGT, van Dam H, Lindeman JH, Goumans MJ, ten Dijke P. Inflammation induces endothelial-to-mesenchymal transition and promotes vascular calcification through downregulation of BMPR2. *J Pathol*. 2019;247:333–346. doi: 10.1002/path.5193
51. Shin J, Hong J, Edwards-Glenn J, Krukovets I, Tkachenko S, Adelus ML, Romanoski CE, Rajagopalan S, Podrez E, Byzova TV, et al. Unraveling the role of sex in endothelial cell dysfunction: evidence from lineage tracing mice and cultured cells. *Arterioscler Thromb Vasc Biol*. 2024;44:238–253. doi: 10.1161/ATVBAHA.123.319833
52. Schindelin J, Arganda-Carreras I, Frise E, Kaynig V, Longair M, Pietzsch T, Preibisch S, Rueden C, Saalfeld S, Schmid B, et al. Fiji: an open-source platform for biological-image analysis. *Nat Methods*. 2012;9:676–682. doi: 10.1038/nmeth.2019
53. Dobin A, Davis CA, Schlesinger F, Drenkow J, Zaleski C, Jha S, Batut P, Chaisson M, Gingeras TR. STAR: ultrafast universal RNA-seq aligner. *Bioinformatics*. 2013;29:15–21. doi: 10.1093/bioinformatics/bts635
54. Li B, Dewey CN. RSEM: accurate transcript quantification from RNA-seq data with or without a reference genome. *BMC Bioinf*. 2011;12:323. doi: 10.1186/1471-2105-12-323
55. Ritchie ME, Phipson B, Wu D, Hu Y, Law CW, Shi W, Smyth GK. limma powers differential expression analyses for RNA-sequencing and microarray studies. *Nucleic Acids Res*. 2015;43:e47. doi: 10.1093/nar/gkv007
56. Kuleshov MV, Jones MR, Rouillard AD, Fernandez NF, Duan Q, Wang Z, Koplev S, Jenkins SL, Jagodnik KM, Lachmann A, et al. Enrichr: a comprehensive gene set enrichment analysis web server 2016 update. *Nucleic Acids Res*. 2016;44:W90–W97. doi: 10.1093/nar/gkw377
57. Pérez-Silva JG, Araujo-Voces M, Quesada V. nVenn: generalized, quasi-proportional Venn and Euler diagrams. *Bioinformatics*. 2018;34:2322–2324. doi: 10.1093/bioinformatics/bty109
58. Zhang YE. Non-Smad signaling pathways of the TGF-β family. *Cold Spring Harb Perspect Biol*. 2017;9:a022129. doi: 10.1101/cshperspect.a022129
59. Mahler GJ, Farrar EJ, Butcher JT. Inflammatory cytokines promote mesenchymal transformation in embryonic and adult valve endothelial cells. *Arterioscler Thromb Vasc Biol*. 2013;33:121–130. doi: 10.1161/ATVBAHA.112.300504
60. Yoshimatsu Y, Wakabayashi I, Kimuro S, Takahashi N, Takahashi K, Kobayashi M, Maishi N, Podyma-Inoue KA, Hida K, Miyazono K, et al. TNF-α enhances TGF-β-induced endothelial-to-mesenchymal transition via TGF-β signal augmentation. *Cancer Sci*. 2020;111:2385–2399. doi: 10.1111/cas.14455
61. Adjuto-Saccone M, Soubeyran P, Garcia J, Audebert S, Camoin L, Rubis M, Roques J, Binétruy B, Iovanna JL, Tournaire R. TNF-α induces endothelial-mesenchymal transition promoting stromal development of pancreatic adenocarcinoma. *Cell Death Dis*. 2021;12:649. doi: 10.1038/s41419-021-03920-4
62. Lopez-Mejia IC, de Toledo M, Chavey C, Lapasset L, Cavelier P, Lopez-Herrera C, Chebli K, Fort P, Beranger G, Fajas L, et al. Antagonistic functions of LMNA isoforms in energy expenditure and lifespan. *EMBO Rep*. 2014;15:529–539. doi: 10.1002/embr.201338126
63. Hamczyk MR, del Campo L, Andrés V. Aging in the cardiovascular system: lessons from Hutchinson-Gilford progeria syndrome. *Annu Rev Physiol*. 2018;80:27–48. doi: 10.1146/annurev-physiol-021317-121454
64. Osorio FG, Navarro CL, Cadiñanos J, López-Mejía IC, Quirós PM, Bartoli C, Rivera J, Tazi J, Guzmán G, Varela I, et al. Splicing-directed therapy in a new mouse model of human accelerated aging. *Sci Transl Med*. 2011;3:106ra107. doi: 10.1126/scitranslmed.3002847
65. Sörensen I, Adams RH, Gossler A. DLL1-mediated Notch activation regulates endothelial identity in mouse fetal arteries. *Blood*. 2009;113:5680–5688. doi: 10.1182/blood-2008-08-174508
66. Wang Y, Nakayama M, Pitulescu ME, Schmidt TS, Bochenek ML, Sakakibara A, Adams S, Davy A, Deutsch U, Lüthi U, et al. Ephrin-B2 controls VEGF-induced angiogenesis and lymphangiogenesis. *Nature*. 2010;465:483–486. doi: 10.1038/nature09002
67. Clausen BE, Burkhardt C, Reith W, Renkawitz R, Förster I. Conditional gene targeting in macrophages and granulocytes using LysMcre mice. *Transgenic Res*. 1999;8:265–277. doi: 10.1023/a:1008942828960